

Discovery of Novel Hybrids Containing Clioquinol–1-benzyl-1,2,3,6-tetrahydropyridine as Multi-Target-Directed Ligands (MTDLs) Against Alzheimer’s Disease

Xinnan Li,^{†,#} Tiantian Li,^{‡,#} Pengfei Zhang,[†] Xinuo Li,[†] Li Lu,[‡] Yuan Sun,[†] Bocheng Zhang,[‡] Stephanie Allen,[‡] Lisa White,[‡] James Phillips,[§] Zheyang Zhu,^{‡,*} Hequan Yao,^{†,*} Jinyi Xu^{†,*}

[†] State Key Laboratory of Natural Medicines and Department of Medicinal Chemistry, China Pharmaceutical University, 24 Tong Jia Xiang, Nanjing 210009, P. R. China

[‡] School of Pharmacy, The University of Nottingham, University Park Campus, Nottingham NG7 2RD, UK

[§] School of Pharmacy, University College London, London WC1N 1AX, UK

AUTHOR INFORMATION

Corresponding Authors

*E-mail: Zheyang.Zhu@nottingham.ac.uk (for Z.Z.)

*E-mail: cpuhyao@126.com (for H.Y.)

*E-mail: jinyixu@china.com (for J.X.)

Author Contributions

[#]X.L. and T.L. contributed equally to this work.

Abstract

Based on the multitarget strategy, a series of novel clioquinol-1-benzyl-1,2,3,6-tetrahydropyridine hybrids were identified for the potential treatment of Alzheimer's disease (AD). Biological evaluation *in vitro* revealed that these hybrids exhibited significant inhibitory activities toward acetylcholinesterase (AChE). The optimal compound, **19n**, exhibited excellent AChE inhibitory potency ($IC_{50} = 0.11 \mu M$), appropriate metal chelating functions, modulation of AChE- and metal-induced $A\beta$ aggregation, neuroprotection against okadaic acid-induced mitochondrial dysfunction and ROS damage, and interesting properties that reduced p-Tau levels in addition to no toxicity on SH-SY5Y cells observed at a concentration up to $50 \mu M$. Most importantly, compound **19n** was more well tolerated ($>1200 \text{ mg/kg}$) than donepezil ($LD_{50} = 28.124 \text{ mg/kg}$) *in vivo*. Moreover, compound **19n** demonstrated marked improvements in cognitive and spatial memory in two AD mice models (scopolamine-induced and $A\beta_{1-42}$ -induced) and suppressed inflammation induced by $A\beta_{1-42}$ in the cortex. The multifunctional profiles of compound **19n** demonstrate that it deserves further investigation as a promising lead in the development of innovatively multifunctional drugs for Alzheimer's disease.

Keywords: Clioquinol, Donepezil, Metal-chelating, Acetylcholinesterase, Alzheimer's disease.

1. Introduction

Alzheimer's disease (AD) is one of the most common causes of dementia resulting in significant malfunctions in memory, thinking, and behavior [1]. With the world's aging population, there is a growing health care burden of epidemic proportions [2]. Despite significant effort and investment, the quest to develop effective disease-modifying medicines to prevent or treat this devastating and complex disease has resulted in many failures [3]. With a rapidly rising incidence and mortality rate, AD has surpassed cardiovascular disease and cancer to become the third leading cause of death in older people [4]. The World Alzheimer Report 2019 pointed out that with the

continuous acceleration of the aging population, the number of AD patients worldwide had exceeded 50 million, and was expected to reach 152 million by 2050.

AD is a neurodegenerative disease caused by a combination of genetic factors, endogenous factors, exogenous environment, and many other risk factors. Its main pathological features include 1. Extracellular self-aggregation of $A\beta$ to form cytotoxic $A\beta$ oligomers and fibrils; 2. Hyper-phosphorylation of tau protein accumulated in the cell to form neurofibrillary tangles (NFTs); 3. Neuroinflammation and loss of synapses; 4. Impaired cholinergic conduction; 5. Oxidative stress and mitochondrial dysfunction; 6. Intracellular calcium overload [5-8].

The pathogenesis of AD is extremely complex. Several hypotheses have been proposed, including the cholinergic injury hypothesis, $A\beta$ toxicity hypothesis, hyperphosphorylation of tau protein hypothesis, metal ion disorder hypothesis, oxidative stress, and inflammation hypothesis [9]. One of the most widely accepted hypotheses is the cholinergic hypothesis, which is related to the observation that AD is characterized by a lack of the neurotransmitter acetylcholine (ACh) [10, 11]. The greatly reduced level of ACh in the synaptic site of the central nervous system is an important feature of AD, and acetylcholinesterase (AChE) inhibitors can prevent AChE from destroying ACh, so far only four AChE inhibitors, tacrine (**1**), donepezil (**2**), rivastigmine (**3**) and galantamine (**4**) (Fig. 1), are approved by the US Food and Drug Administration (FDA) for the treatment of the symptoms associated with mild to advanced AD. Among these drugs, tacrine was discontinued due to concerns linked to hepatotoxicity [12-14]. As a result, the cholinergic hypothesis and approved drugs have led to a high level of interest in AChE and AChE inhibitors (AChEIs) in the field of AD [15], with the single-target strategy aiming at AChE and multi-target strategy involving AChE and another target, which becomes common perspective in new drug design for the potential treatment of AD [16].

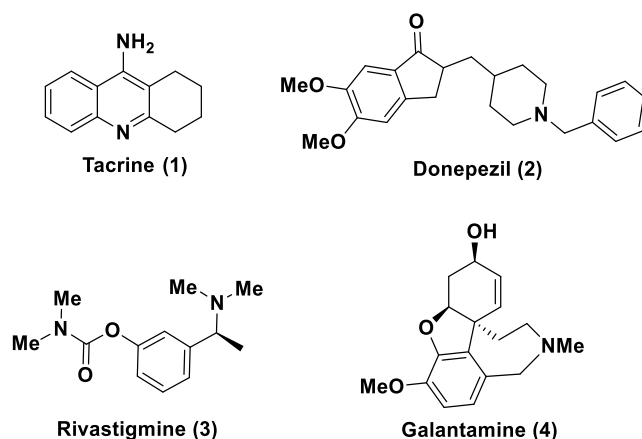


Fig. 1. FDA approved AChE inhibitors for the treatment of AD.

Metal ions are involved in important biological processes such as signal transmission, catalysis, protein structure stabilization, and metabolism [17, 18]. Recent studies showed that abnormally high concentrations of copper, iron, and zinc ions are present in the brain tissue of AD patients, such as the areas of hippocampus, tonsil olfactory bulb, and neocortex [19]. Previous studies revealed that metal ions co-exist in amyloid plaques in the brain tissues of AD patients [20]. In addition, excessive metal ions can cause oxidative stress in the brain, further aggravating the condition of AD. Therefore, metal chelating agents are considered a potential option for the treatment of AD by stabilizing the level of bio-metals in the brain [21, 22].

As the development of single-target anti-AD drugs continues to fail in recent years, due to the complex pathogenesis of AD, with various risk factors interconnecting and influencing each other, resulting in a disease network. Single-target therapy is difficult to effectively control and cure AD, therefore, the study of multi-target directed ligands (MTDLs) targeting the network of AD pathogenesis may be a more effective approach [7, 16, 23, 24]. Given the importance of AChE and bio-metals in the treatment of AD, the design of MTDLs with AChE inhibition and ion chelating ability is receiving much attention in recent years. Yan and co-workers reported a series of novel compounds by fusing the AChEI donepezil with curcumin [25]. The optimal compound showed potent AChE inhibition ($IC_{50} = 187$ nM), metal-chelating ability with Cu^{2+} and Fe^{2+} . In addition, by fusing tacrine with pyrimidone, our group identified a series of novel hybrids with excellent dual AChE/GSK-3 β inhibition, of which, the most promising

compound possesses multiple anti-AD profiles with benign safety and drug-like properties [11].

Donepezil is an AChE inhibitor approved by the FDA for the treatment of AD in 1996. The benzyl piperidine fragment in donepezil is the key pharmacophore, which can effectively bind the catalytic anionic site (CAS) in AChE. In our previous studies, we isolated a structurally unique natural polyphenolic compound (\pm)-7,8-Dihydroxy-3-methyl-isochroman-4-one [(\pm)-XJP, **5**] from banana (*Musa sapientum L.*) peel, which displayed antihypertensive, anti-oxidant, and anti-inflammatory activities [26-29]. These results attracted our interest in further exploration and optimization of pharmacophore (\pm)-XJP. Through modifications of (\pm)-XJP and its derivatives, we successfully obtained several series of new molecules with excellent AChE inhibitory activity and anti-AD effects [30-33]. Moreover, by combining the benzylpiperidine fragment of donepezil with the (\pm)-XJP skeleton, we further synthesized a potent AChE inhibitor **6** with nanomolar activity bearing 1-benzyl-1,2,3,6-tetrahydropyridine ring (Fig. 2).

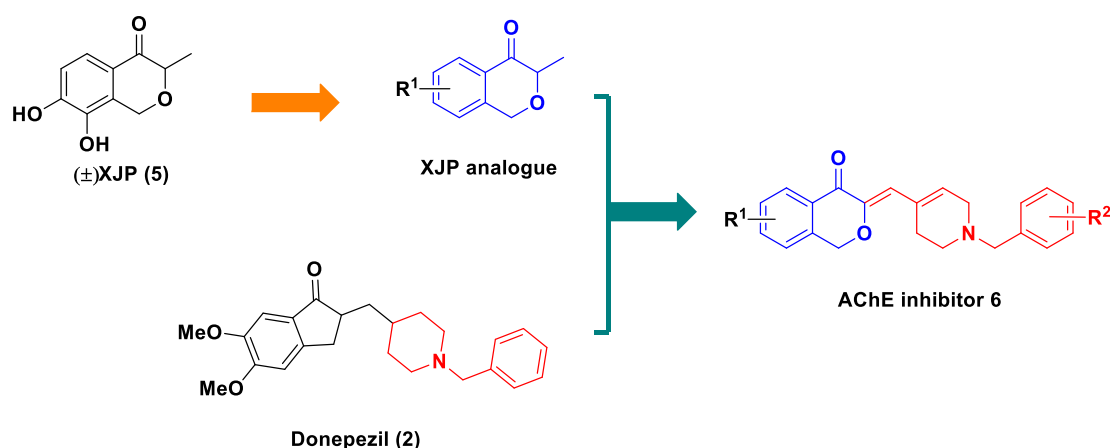


Fig. 2. Strategy for the design of AChE inhibitor **6** in our previous work.

Clioquinol (**7**, Fig. 3) and its analog PBT-2 (**8**, Fig. 3) have the ability to regulate the level of metal ions and reduce the level of A β in plasma, thereby showing good effects on cognitive and memory improvement [34]. The 8-hydroxyquinoline skeleton in the structure plays a key role in the metal chelating function. In addition to metal chelation,

it also has many excellent properties such as blood-brain barrier (BBB) permeability, antioxidant capacity, and resistance to Cu(II)-induced A β aggregation [34].

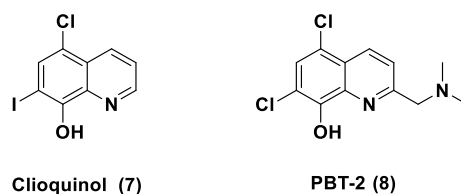


Fig. 3. The structures of clioquinol and PBT-2.

As our continuous interests in discovering and developing novel XJP derivatives as potential therapeutic anti-AD agents, we hypothesize that the design of new hybrids from the group with AChE inhibitory activity and moiety with metal ion chelating ability to produce the novel hybrids with potent activities against AD based on the multitarget strategy. Herein, we report a series of novel MTDLs containing clioquinol–1-benzyl-1,2,3,6-tetrahydropyridine (**19a-p,20a-p**) with both potent AChE inhibitory activity and metal ion chelating ability by fusing the pharmacophore of AChE inhibitor **6** with skeleton of clioquinol (Fig. 4).

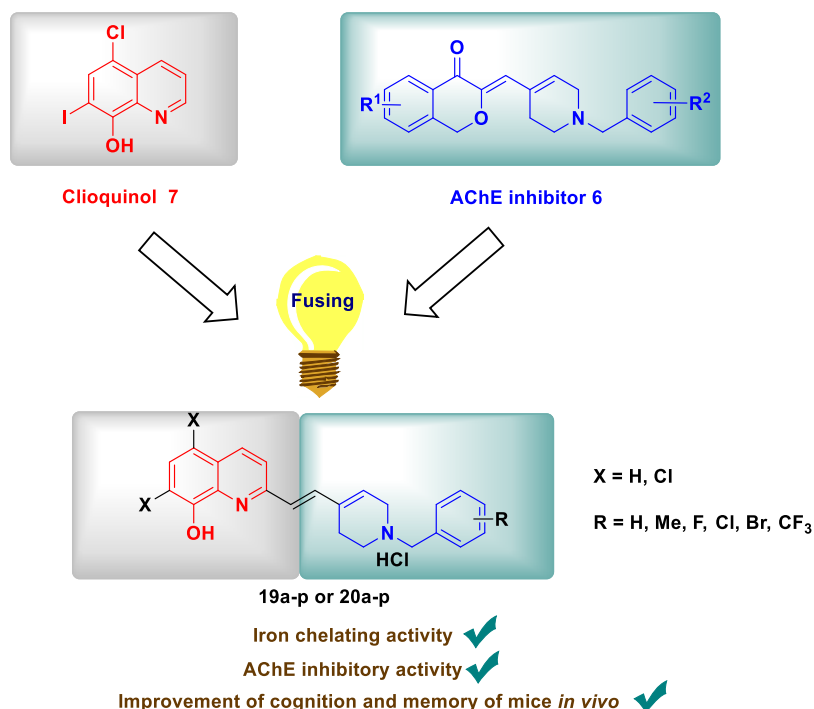
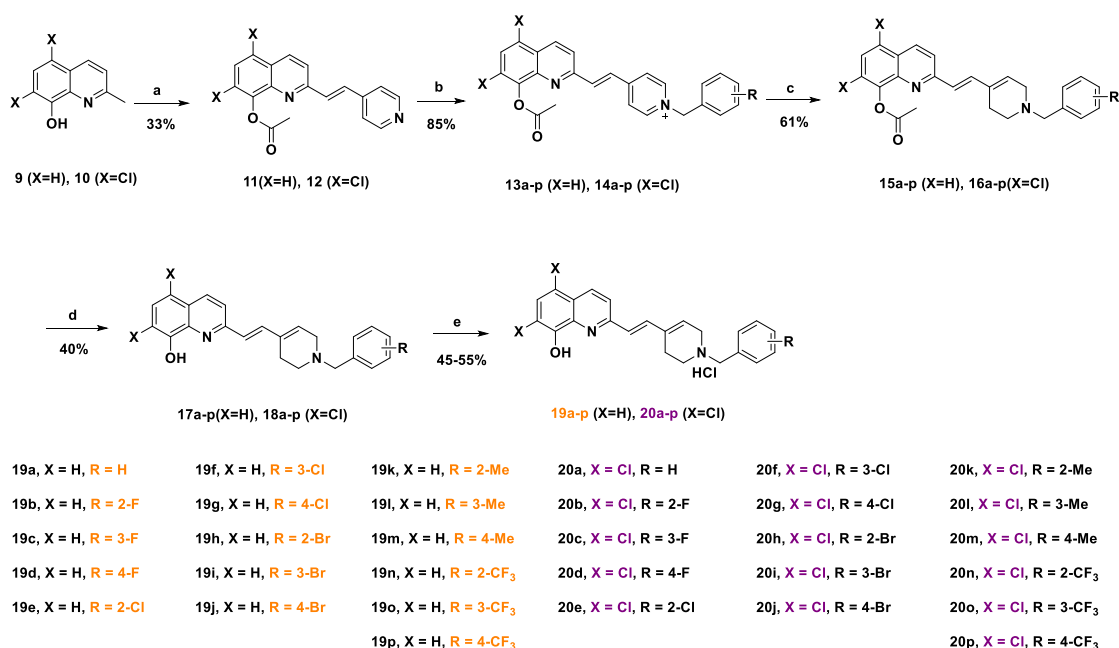


Fig. 4. Strategy for the design of novel anti-AD MTDLs (**19a-p, 20a-p**).

2. Results and discussion

2.1 Synthesis

The synthetic routes to the target compounds (**19a-p** and **20a-p**) were depicted in Scheme 1. Starting with commercially available **9** and **10**, which reacted with 4-pyridinecarboxaldehyde in dry acetic anhydride under argon atmosphere to yield the key intermediates **11** and **12**. Then **11** and **12** reacted with different substituted benzyl bromides to give the intermediates **13a-p** and **14a-p**, followed by a reductive reaction by sodium borohydride in ethanol solution to obtain **15a-p** and **16a-p**. Deacetylation with potassium carbonate provided the intermediates **17a-p** and **18a-p**. Finally, **17a-p** and **18a-p** reacted with hydrogen chloride to obtain the target compounds **19a-p** and **20a-p**.

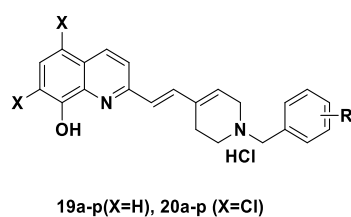


Scheme 1. Synthetic approach to compounds **19a-p** and **20a-p**. *Reagents and conditions:* (a) 4-pyridinecarboxaldehyde, acetic anhydride, 60 °C, 10 h; (b) substituted benzyl bromide, MeCN, reflux, 3-5 h; (c) NaBH₄, EtOH, 0 °C, 1 h; (d) K₂CO₃, MeOH, r.t., 30 min; (e) HCl, EA, 0 °C, 1 h.

2.2 Inhibition of AChE and structure-activity relationship

The inhibitory activity against AChE of all target compounds was assessed in electrophorus electricus AChE (eeAChE) using Ellman's spectrophotometric method with some minor modifications [35], donepezil was used as the positive control. The anti-AChE activities for all target compounds expressed as IC₅₀ values are provided in Table 1. The results in Table 1 indicated that most of the target compounds exhibited good potent inhibitory activities against AChE. Among two series of compounds **19a-19p** (X = H) and **20a-20p** (X = Cl), compounds **19n** (IC₅₀ = 0.11 μM) and **20l** (IC₅₀ = 0.25 μM), which bear a 2-trifluoromethyl or 3-methyl on the benzyl moiety, demonstrated better activities than the other analogs in the series of compounds. In the first series of compounds **19a-19p**, the predominant substitutions among different substituents in the benzyl group are 2-CF₃ (**19n**), 2-F (**19b**), 3-Cl (**19f**), 4-Br (**19j**), and 4-Me (**19m**). In the second series of compounds **20a-20p**, the predominant substitutions among different substituents in the benzyl group are 4-CF₃ (**20p**), 4-F (**20d**), 3-Cl (**20f**), 3-Br (**20i**), and 3-Me (**20l**). In general, the introduction of substituents on the benzene ring is beneficial to increasing the inhibitory activity against AChE, and the introduction of dichloro-substituent on the quinoline ring is beneficial to reducing the amplitude of the activity fluctuation of the compounds.

Table 1. *In vitro* AChE inhibitory activity of compounds **19a-p** and **20a-p**



Compd.	X	R	eeAChE IC ₅₀ (μM) ^a	Compd.	X	R	eeAChE IC ₅₀ (μM) ^a
19a	H	H	1.11 ± 0.12	20a	Cl	H	2.31 ± 0.16
19b	H	2-F	0.57 ± 0.23	20b	Cl	2-F	0.29 ± 0.03
19c	H	3-F	0.72 ± 0.11	20c	Cl	3-F	0.52 ± 0.07
19d	H	4-F	1.66 ± 0.30	20d	Cl	4-F	0.27 ± 0.13
19e	H	2-Cl	1.29 ± 0.41	20e	Cl	2-Cl	0.41 ± 0.15

19f	H	3-Cl	0.75 ± 0.15	20f	Cl	3-Cl	0.33 ± 0.26
19g	H	4-Cl	3.05 ± 1.01	20g	Cl	4-Cl	0.62 ± 0.16
19h	H	2-Br	0.49 ± 0.33	20h	Cl	2-Br	0.54 ± 0.03
19i	H	3-Br	1.53 ± 0.12	20i	Cl	3-Br	0.32 ± 0.02
19j	H	4-Br	0.26 ± 0.02	20j	Cl	4-Br	0.64 ± 0.02
19k	H	2-Me	0.40 ± 0.08	20k	Cl	2-Me	0.56 ± 0.05
19l	H	3-Me	0.43 ± 0.11	20l	Cl	3-Me	0.25 ± 0.12
19m	H	4-Me	0.26 ± 0.22	20m	Cl	4-Me	0.54 ± 0.03
19n	H	2-CF ₃	0.11 ± 0.10	20n	Cl	2-CF ₃	0.34 ± 0.05
19o	H	3-CF ₃	0.55 ± 0.21	20o	Cl	3-CF ₃	0.70 ± 0.19
19p	H	4-CF ₃	0.32 ± 0.06	20p	Cl	4-CF ₃	0.28 ± 0.04
Donepezil			0.02 ± 0.03				

^a Results are expressed as the mean of at least three experiments.

2.3 Docking studies of compounds **19n** and **20l** with AChE.

In order to assess the ligand-enzyme interactions, docking simulations were performed using the Glide program of the Schrodinger. The X-ray crystal structure of human AChE (PDB entry 4EY7) was acquired from the PDB. Based on the *in vitro* inhibitory results, compounds **19n** and **20l** were selected as the typical ligands for evaluation. The docking results were shown in Fig. 5 (A, B, C), and it can be found that the binding modes of **19n** and **20l** with AChE were similar, but there were some differences. The benzyl-tetrahydropyridine moiety of both compounds located in the CAS site of the active pocket, while the quinoline moiety occupied the PAS site of the active pocket and formed π - π interaction with Trp-286 within the active pocket. There were two π - π interactions and no strong secondary bonds (e.g. hydrogen, halogen bonds) were formed. The main difference in binding to the target was the benzene ring at the end of benzyl, where **19n** formed one π - π interaction with Trp-86, while **20l** formed two π - π interactions with Trp-86. In docking score, **19n** (IC₅₀ = 0.11 μ M) scored -11.244, which was better than **20l** (IC₅₀ = 0.25 μ M) of -10.580, this was consistent with the results of their actual inhibitory activity assay. Considering that the π - π interaction was

a weaker secondary bond, we inferred that the π - π interaction and Van der Waals force together constitute the active basis of these compounds, and the Van der Waals force occupies a larger proportion.

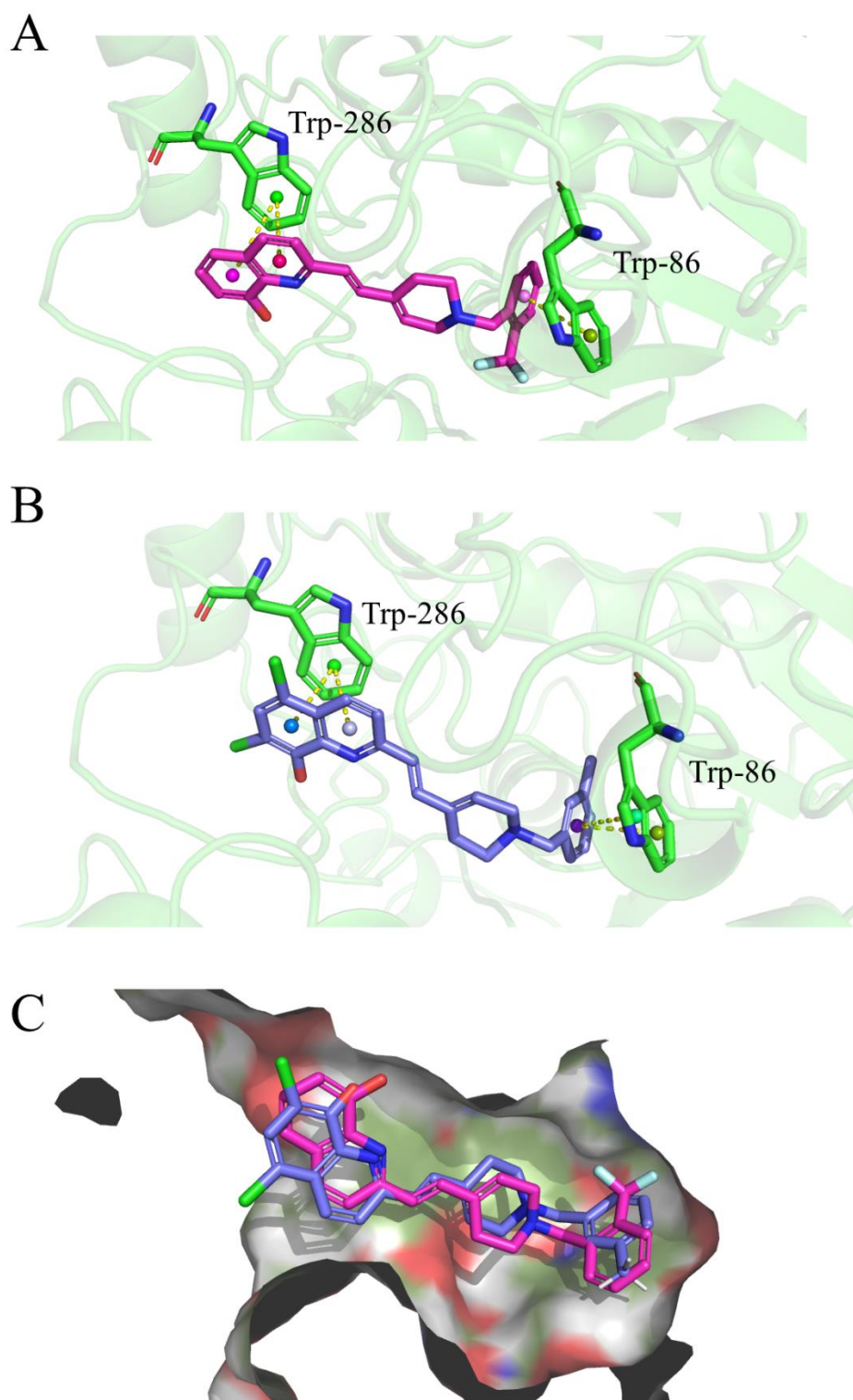


Fig. 5. Proposed binding models of **19n** (A) or **20l** (B) with AChE (PDB code: 4EY7). π - π interactions were shown as yellow dotted lines. (A) Relative position of **19n** (shown

in purple) in the active pocket of AChE. (B) Relative position of **20l** (shown in blue) in the active pocket of AChE. (C) Relative positions of **19n** (shown in purple) and **20l** (shown in blue) in the active pocket of AChE.

2.4 Kinetic study of compound **19n** for the inhibition of AChE

In order to investigate the mechanism of 1-benzyl-1,2,3,6-tetrahydropyridine-clioquinol derivatives against AChE, we performed the kinetic characterization of AChE inhibition for the most potent compound **19n** to evaluate the inhibition type. The graphical presentation of the steady-state inhibition data shown in Fig. 6 demonstrated that the intersection point of the Lineweaver–Burk reciprocal plot was located in the second quadrant, which indicated that the inhibition mode of compound **19n** was mixed-type inhibition.

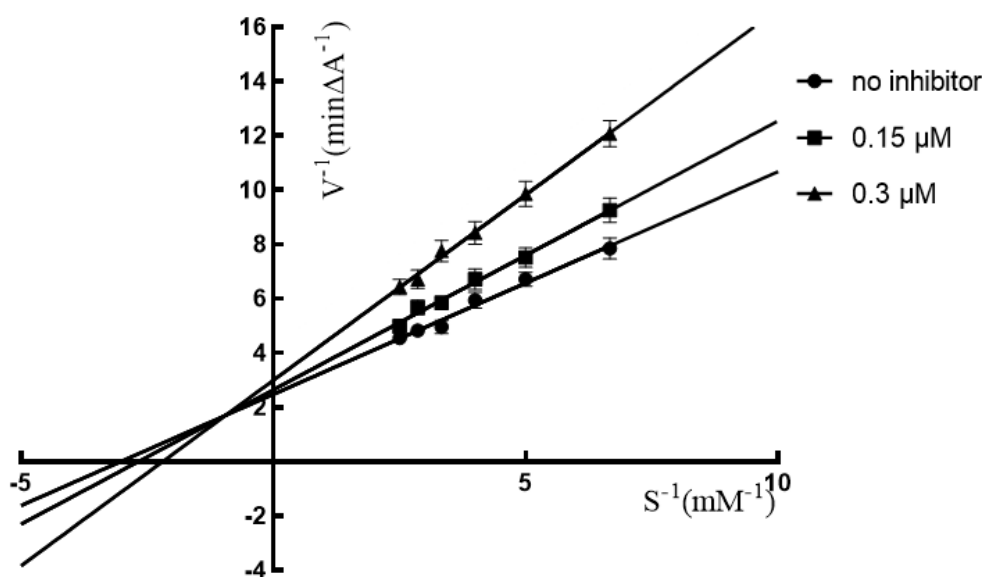


Fig. 6. Lineweaver-Burk plot on two distinct concentrations of **19n** for AChE.

2.5 Metal-chelating properties of compounds **19n** and **20l**

The chelating ability of compounds **19n** and **20l** towards biologically relevant metal ions such as Cu^{2+} , Fe^{2+} , Fe^{3+} , Zn^{2+} , and Al^{3+} was investigated by UV-Vis spectroscopy [36]. The electronic spectra of compound **19n** in methanol changed significantly in the

presence of Cu^{2+} , Fe^{2+} , Fe^{3+} , Zn^{2+} , and Al^{3+} (Fig. 7A). Upon addition of CuCl_2 , the curve was red-shifted (peak at 293 nm to 307 nm), indicating the formation of the **19n**- Cu^{2+} complex (Fig. S1A), while the addition of FeSO_4 , FeCl_3 , ZnCl_2 , and AlCl_3 the curve was also shifted (Fig. S1B-E), indicating that **19n** has the ability to chelate all five ions: Cu^{2+} , Fe^{2+} , Fe^{3+} , Zn^{2+} , and Al^{3+} . For compound **20l**, the absorption peaks were red-shifted and shifted towards 308 nm (Fig. S2A) and 298 nm (Fig. S2D) when Cu^{2+} and Fe^{2+} were added respectively. The absorption peaks were blue-shifted and slightly shifted towards 296 nm when Al^{3+} was added (Fig. S2C), however, the absorption peaks remained at 297 nm when Zn^{2+} and Fe^{3+} were added (Fig. S2B/E). These results indicate that compound **20l** has the ability to chelate Cu^{2+} , Fe^{2+} and Al^{3+} , but not Zn^{2+} and Fe^{3+} (Fig. 7B). In order to determine the stoichiometry of the **19n**- Cu^{2+} and **20l**- Cu^{2+} complexes, the total concentration of compound and Cu^{2+} was fixed at 100 μM and the concentration of the compound in different solutions was increased in a 5% gradient from 0 to 100%. After the solutions were prepared, they were incubated at 37°C for 1 hour and tested for absorbance (**19n** was tested at 307 nm and **20l** at 308 nm). For compound **19n**, two straight lines intersected at $X = 0.54$, revealing a 1:1 stoichiometry for the **19n**- Cu^{2+} complex (Fig. 7C). For compound **20l**, two straight lines intersect at $X = 0.65$, revealing a 2:1 stoichiometry for the complex **20l**- Cu^{2+} (Fig. 7D).

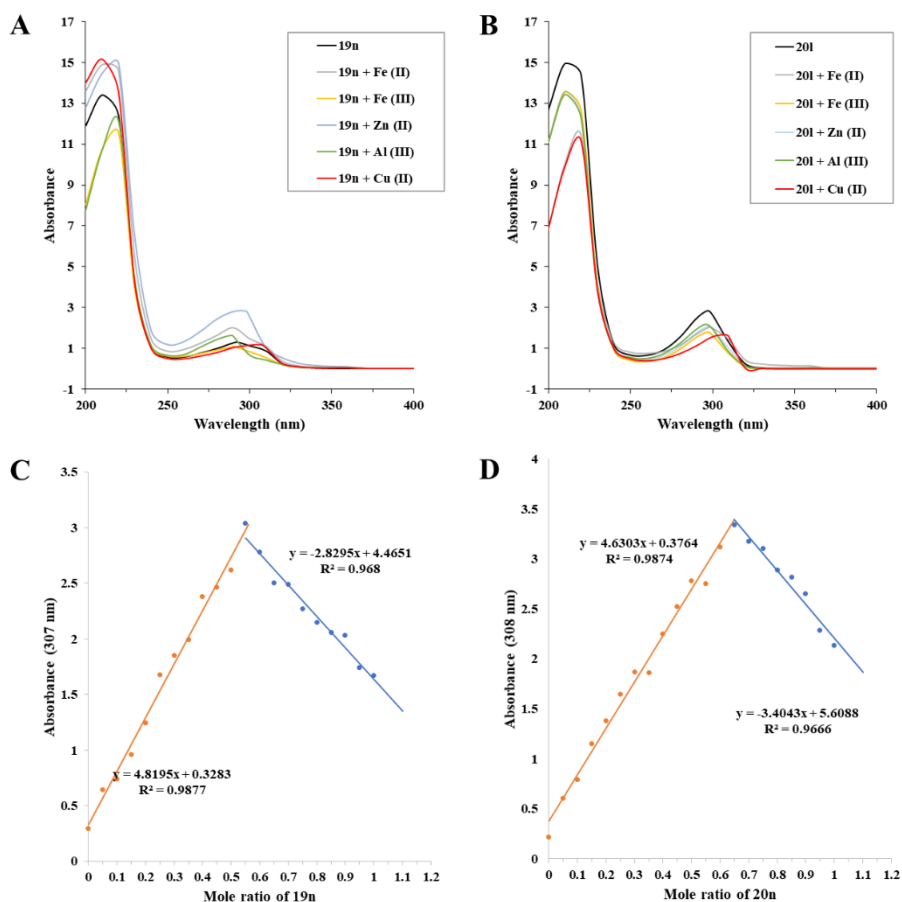


Fig. 7. (A) UV absorbance spectrum of **19n** (40 μM) alone or in the presence of FeSO_4 (20 μM), FeCl_3 (20 μM), ZnCl_2 (20 μM), AlCl_3 (20 μM) or CuSO_4 (20 μM) in dry methanol. (B) UV absorbance spectrum of **20l** (40 μM) alone or in the presence of FeSO_4 (20 μM), FeCl_3 (20 μM), ZnCl_2 (20 μM), AlCl_3 (20 μM) or CuSO_4 (20 μM) in dry methanol. (C) Determination of the stoichiometry of complex Cu^{2+} -**19n**. (D) Determination of the stoichiometry of complex Cu^{2+} -**20l**.

2.6 Modulation of Cu^{2+} -Induced $\text{A}\beta$ Aggregation by Compound **19n**.

The effects of compound **19n** on Cu^{2+} -induced $\text{A}\beta$ aggregation was investigated using the ThT assay, and the morphological changes of $\text{A}\beta$ species were then examined using a transmission electron microscopy (TEM) assay [36]. In the ThT assay, after a 24 h incubation, Cu^{2+} -induced $\text{A}\beta$ aggregation significantly increased, while compounds **19n** and clioquinol (CQ), not donepezil (Don), displayed remarkable effects on the modulation of Cu^{2+} -induced $\text{A}\beta$ aggregation (Fig. 8A), albeit compounds **19n**, or CQ showed no effect on $\text{A}\beta$ self-aggregation without the presence of Cu^{2+} (Fig. 8A). The visually morphological changes of the $\text{A}\beta$ samples were further observed by TEM (Fig. 8B). The TEM images showed that the Cu^{2+} -treated fresh $\text{A}\beta$ sample produced more fibrils compared to the untreated sample (Fig. 8B, sequences 2 and 3). When compounds **19n** and CQ were incubated with the sample, $\text{A}\beta$ aggregates clearly decreased and fewer $\text{A}\beta$ fibrils were detected (Fig. 8B, sequences 4, 5); however, donepezil had no comparable effect (Fig. 8B, sequences 6). These TEM findings supported the results obtained from the ThT assay and jointly proved that compound **19n** can indeed inhibit Cu^{2+} -induced $\text{A}\beta$ aggregation.

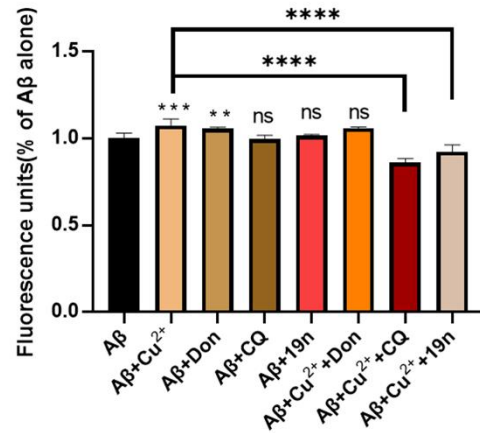
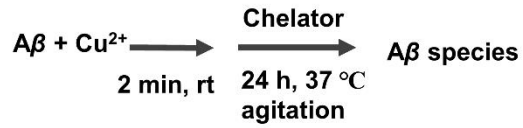
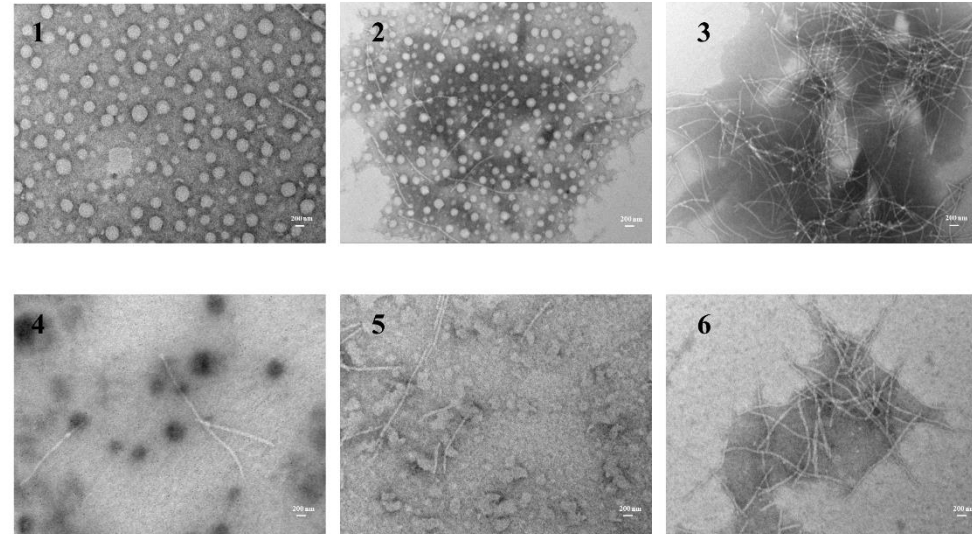
A**B**

Fig. 8. Modulation of anti-AD compounds on Cu^{2+} -induced $A\beta_{1-42}$ aggregation. (A) The fluorescence intensity of the ThT binding assay ($n=8$), data are expressed as the mean \pm SD. Statistical significance was analyzed by ANOVA: * $p < 0.05$, ** $p < 0.01$, *** $p < 0.001$, **** $p < 0.0001$. (B) TEM image analysis of the inhibition of compounds on Cu^{2+} -induced $A\beta_{1-42}$ aggregation. Serial numbers indicate the following: (1) fresh $A\beta_{1-42}$, (2) $A\beta_{1-42}$ alone, (3) $A\beta_{1-42} + Cu^{2+}$, (4) $A\beta_{1-42} + Cu^{2+} + 19n$, (5) $A\beta_{1-42} + Cu^{2+} + CQ$, (6) $A\beta_{1-42} + Cu^{2+} + Don$. Experimental conditions were as follows: $A\beta_{1-42}$ (25 μM); compound/ $A\beta_{1-42}$ / Cu^{2+} = 2:1:1; HEPES (20 mM) and NaCl (150 mM); pH 7.5; 37 °C.

2.7 Compound **19n** inhibited AChE-induced A β aggregation

A β aggregation is a key pathological hallmark of AD. Studies showed that AChE is involved in the A β aggregation and can accelerate the formation of amyloid fibrils. Therefore, AChE inhibitors may prevent or reduce the formation of A β aggregation. Thus, compound **19n** was tested *in vitro* for its ability to inhibit AChE-induced A β aggregation using the thioflavin T (ThT) fluorescence method. Donepezil was used as a positive control compound. The results shown in Fig. 9 demonstrated that compound **19n** effectively inhibits the AChE-induced A β aggregation rate in a dose-dependent manner, and **19n** has a similar potency to donepezil, as the IC₅₀ values indicated in Table 2.

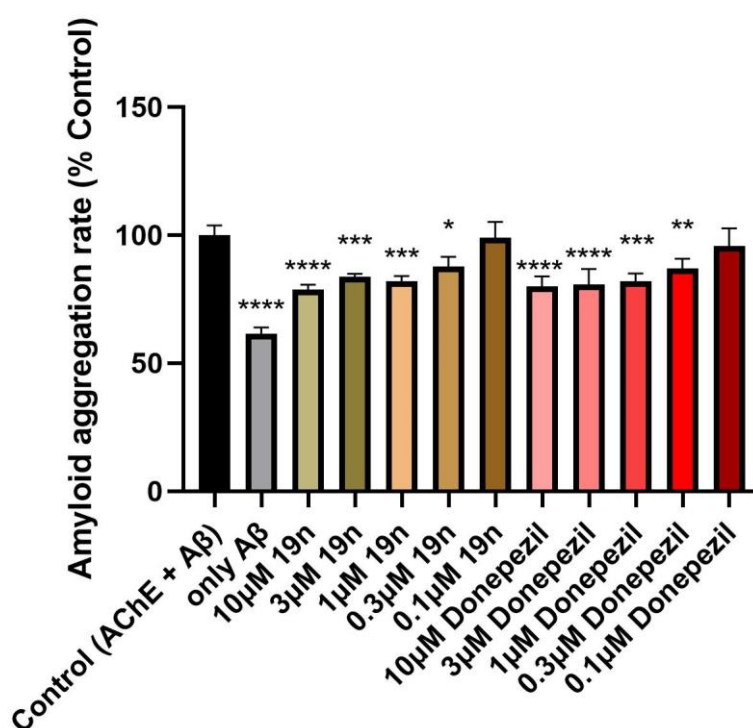


Fig. 9. Reduction in AChE-induced A β aggregation when cells are treated with 0.1 μ M to 10 μ M of **19n** or donepezil for 24 h. Amyloid aggregation rate values are plotted as a percentage of the average value derived from control \pm standard deviation (n=6). Ordinary one-way ANOVA followed by Dunnett's multiple comparisons test was used to compare differences between different groups. *P<0.05; **P<0.01; ***P<0.001; ****P<0.0001.

2.8 Cytotoxic effect of compound **19n** on human neuroblastoma SH-SY5Y cells

Safety is very crucial for drug development, so we investigated the potential toxic effect of **19n** on human neuroblastoma SH-SY5Y cells. As shown in Fig. 10, donepezil was used as a control, the SH-SY5Y cells were exposed to compound **19n** at the concentrations of 1 μM , 20 μM , and 50 μM , respectively for 24 h, and the cell viability was determined by the 3-(4,5-dimethylthiazol-2-yl)-2,5-diphenyl-tetrazolium bromide (MTT) assay. The results suggested that compound **19n** exhibited no statistically significant change in cell viability up to the maximum tested concentration of 50 μM .

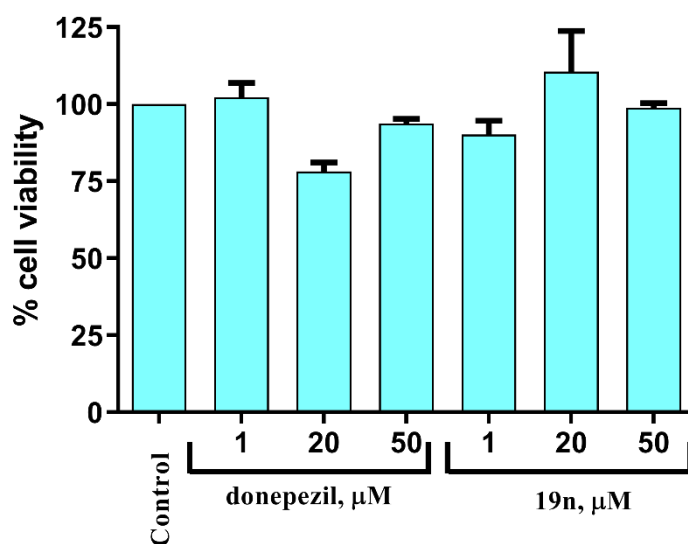


Fig. 10. Cell viability on neuroblastoma SH-SY5Y cells treated with different concentrations of donepezil and **19n** (n=3).

2.9 Compound **19n** inhibited cellular AChE enzymatic activity in human neuroblastoma SH-SY5Y cells

AChE is a key enzyme required for the degradation of acetylcholine in the synaptic cleft. As a main target of action for the anti-AD compounds, we examined the potency of **19n** and donepezil in inhibiting acetylcholinesterase activity in SH-SY5Y cells. Inhibitory activity was examined using Ellman's method following 24 h incubation periods with **19n** and donepezil. Donepezil, a selective and reversible AChE inhibitor approved for AD treatment, was used as a positive control. As shown in Fig. 11,

treatment with either **19n** or donepezil causes a reduction in AChE activity, showing effective inhibition of AChE activity from 0.3 μM or 0.1 μM , up to 10 μM . These results indicate that the test compound **19n** has similar potency toward intra-cellular AChE inhibition with donepezil, as the IC_{50} values indicated in Table 2.

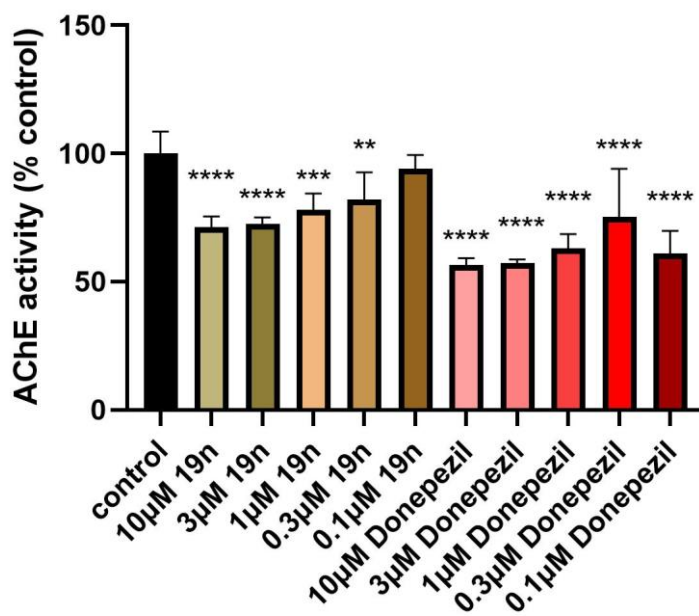


Fig. 11. AChE inhibitory effects in SH-SY5Y cells exposed to different concentrations of test compounds **19n** and donepezil for 24 h. The control contains medium with less than 0.1% DMSO solvent. AChE activity values are plotted as a percentage of the averaged value derived from vehicle-treated control \pm standard deviation ($n=6$). Ordinary one-way ANOVA followed by Dunnett's multiple comparisons test was used to compare differences between different groups. * $P < 0.05$; ** $P < 0.01$; *** $P < 0.001$; **** $P < 0.0001$.

2.10 Compound **19n** protect from okadaic acid-induced mitochondrial dysfunction

Mitochondrial dysfunction is a key pathological factor to results in AD. The okadaic acid (OA) (Fig. 12B) can induce mitochondrial dysfunction as revealed by alteration in calcium ions, reactive oxygen species (ROS) generation, and ATP levels in the brain regions. Previous studies have shown that mitochondrial dysfunction and

memory impairment could be prevented by donepezil treatment [37]. Thus, it is accepted that okadaic acid-induced toxicity is a good model to assess mitochondrial dysfunction occurring in AD pathology. To investigate whether **19n** protects against OA-induced mitochondrial dysfunction, we explored mitochondrial membrane potential (MMP) in SH-SY5Y cells using the JC-1 fluorescent cell-based assay. The healthier mitochondrial function is, the higher ratio of red/green fluorescence intensity would be. As shown in Fig. 12A, cells with 30 nM OA treatment for 24 h caused a reduction in the red/green fluorescence intensity ratio compared to the untreated group. The cells were pre-incubated with the test compound **19n** for 24 h before OA was added and incubated for another 24 h. Fig. 12A shows that pre-treatment of SHSY-5Y cells for 24 hours with **19n** and donepezil caused an increase in red/green fluorescence intensity ratio compared to the cells treated with OA only. These results demonstrated that OA induces mitochondrial damage, and **19n** can effectively protect against this damage, preventing the decrease of MMP from 1 μ M thus showing a neuroprotective effect, with a similar potency to donepezil, as the IC₅₀ values indicated in Table 2.

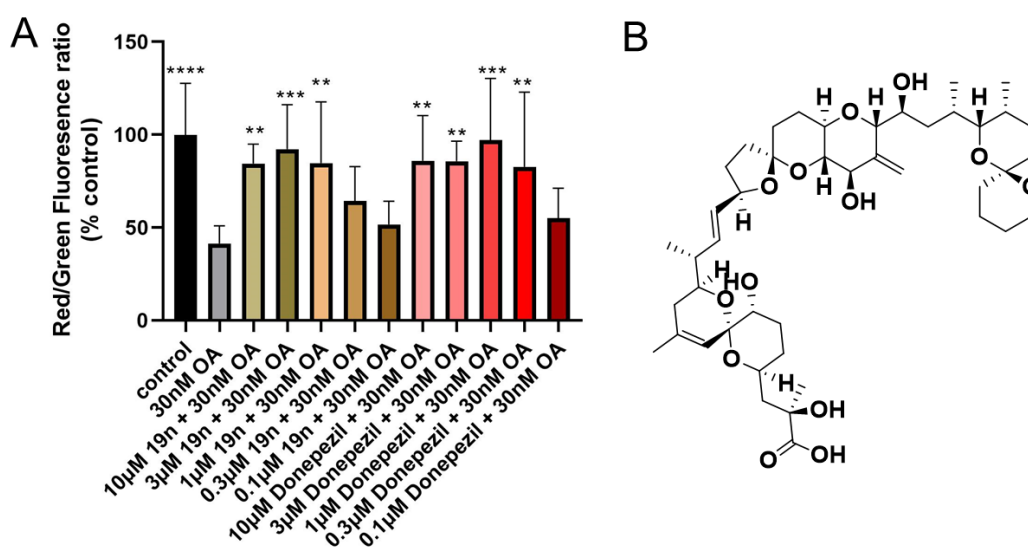


Fig. 12. (A) The ratio of red to green fluorescence following JC-1 assay in the SHYSY-5Y cells, exposed to increasing concentrations of test compound **19n** and positive control donepezil (0.1 μ M – 10 μ M) prior to exposure to 30 nM okadaic acid for an additional 24 h. The Control group contains medium with less than 0.1% DMSO solvent.

The ratio values are plotted as a percentage of the averaged value derived from vehicle-treated control \pm standard deviation (n=6). Ordinary one-way ANOVA followed by Dunnett's multiple comparisons test was used to compare differences between different groups. *P < 0.05; **P < 0.01; ***P < 0.001; ****P < 0.0001. (B) The structure of okadaic acid.

2.11 Compound **19n** protect from okadaic acid-induced ROS damage

To explore the possibility that **19n** protects against OA-induced ROS generation, we measured intracellular ROS levels using the DCF-DA fluorescence assay. As shown in Fig. 13, treatment of SH-SY5Y cells with 30 nM OA for 24 hours increased fluorescence compared to the untreated control group. Fig. 13 shows that pre-treatment of these cells with donepezil and **19n** caused a reduction in DCF fluorescence intensity compared to cells treated with OA only. These results demonstrated that OA induces ROS generation, and **19n** can effectively protect against this effect, preventing the generation of intracellular ROS from 1 μ M, with a similar potency to donepezil, as the IC₅₀ values indicated in Table 2.

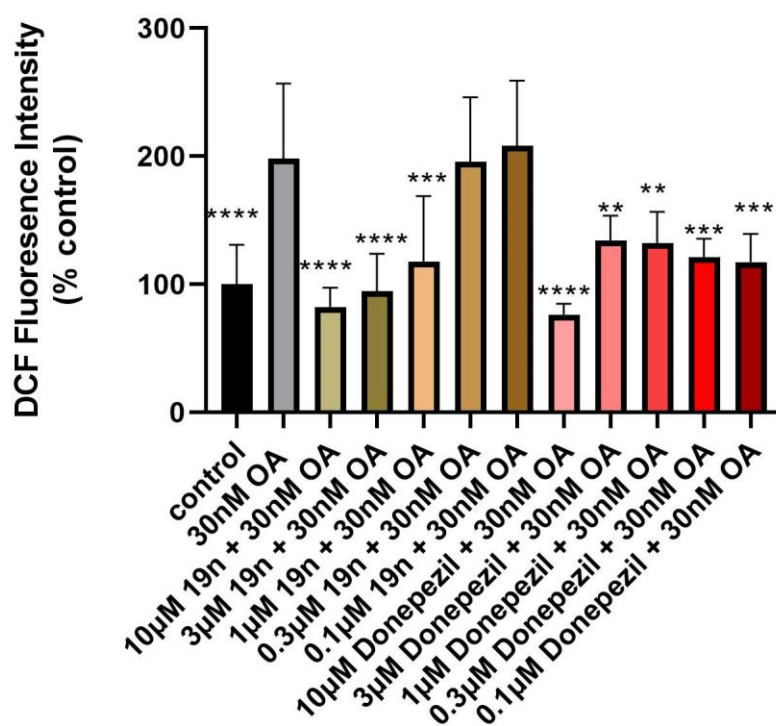


Fig. 13. DCF fluorescence intensity in SH-SY5Y cells, pre-treated for 24 h with increasing concentrations of test compound **19n** and positive control Donepezil, prior to exposure to 30 nM okadaic acid (OA) for another 24 hours. The control group contains medium with less than 0.1% DMSO solvent. Intensity values are plotted as a percentage of the averaged value derived from vehicle-treated control \pm standard deviation (n=6). Ordinary one-way ANOVA followed by Dunnett's multiple comparisons test was used to compare differences between different groups. *P < 0.05; **P < 0.01; ***P < 0.001; ****P < 0.0001.

*2.12 Compound **19n** prevent from GA-induced phosphorylation of tau protein*

Apart from amyloid plaques, another key hallmark of AD pathology is hyperphosphorylation of tau proteins. Glyceraldehyde (GA), an inhibitor of glycolysis, results in glycolytic inhibition, cell apoptosis, and an increase in tau protein phosphorylation. Studies showed GA can increase tau phosphorylation in SH-SY5Y cells [38]. Thus, compound **19n** was tested in SH-SY5Y cells for its ability to inhibit phosphorylation of the tau protein in the neuronal cells using an enzyme-linked immunosorbent assay (ELISA) method. Donepezil was used as a positive control compound. The results shown in Fig. 14 indicated that the phosphorylation ratio of intracellular tau was increased significantly in the 0.7 mM GA treated group compared with the untreated control group. In contrast to the 0.7 mM GA group, compound **19n** presents a significant reduction in p-Tau levels at both the S199 and S396 residues, similar to donepezil, as the IC₅₀ values indicated in Table 2. Therefore, compound **19n** was shown to reverse or prevent from GA-induced phosphorylation of tau protein in SH-SY5Y cells.

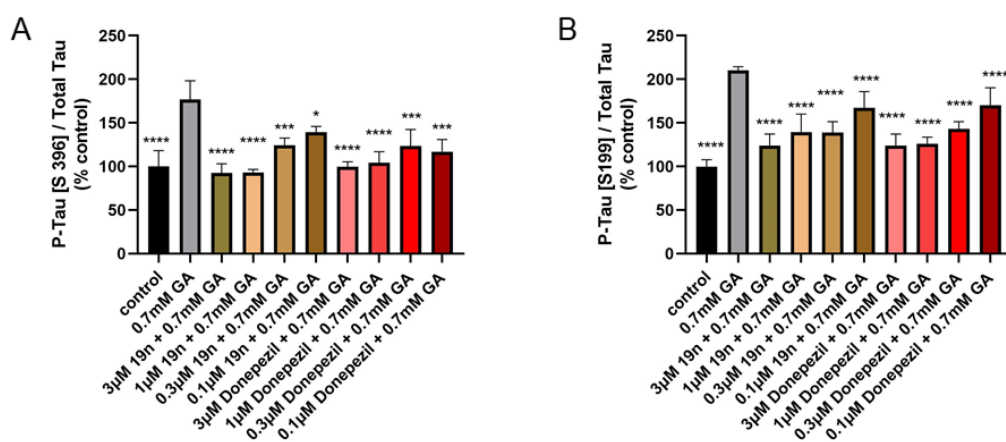


Fig. 14. Quantification of phosphorylation ratio of p-Tau/total tau of GA-treated SH-SY5Y cells after **19n** or donepezil treatment at 0.1 μ M to 3 μ M. The untreated control group is the cells containing a vehicle with less than 0.1% DMSO solvent. Tau ratio values are plotted as a percentage of the averaged value derived from vehicle-treated control \pm standard deviation (n=6). Ordinary one-way ANOVA followed by Dunnett's multiple comparisons test was used to compare differences between different groups. *P<0.05; **P<0.01; ***P<0.001; ****P<0.0001. (A) Phosphorylation ratio of p-Tau/total tau on the S199 residue of tau protein. (B) Phosphorylation ratio of p-Tau/total tau on the S396 residue of tau protein.

Table 2. Summary of IC₅₀ values of compounds **19n** and donepezil obtained from all the cellular assays

IC ₅₀ * values	AChE (nM)	ROS (nM)	MMP (nM)	A β (nM)	p-Tau (S396) (nM)	p-Tau (S199) (nM)
donepezil	198	202	326	1593	35	155
19n	161	213	434	1655	82	138

* The values were calculated by using Graphpad prism 9 following the model of non-linear regression

2.13 ADMET prediction

In silico prediction of absorption, distribution, metabolism, excretion, and toxicity (ADMET) is an important component of evaluating drug properties in the search for

lead compounds and the development of new drugs. ADMETSAR (<http://lmmd.ecust.edu.cn/admetsar2/>) is an open database for predicting the pharmacokinetic properties of lead compounds. The theoretical calculations of ADMET parameters (BBB penetration, human intestinal absorption (HIA), caco-2 permeability, AMES mutagenesis, rat acute toxicity) of compounds (**19h**, **19j**, **19k**, **19l**, **19m**, **19n**, **19p**, **20b**, **20d**, **20f**, **20i**, **20l**, **20n**, **20p**) with IC₅₀ less than 0.5 μM were presented in Table 3. The ADMET properties of these compounds showed good overall performance. The predicted value of BBB penetration is about 90%, indicating excellent BBB penetration. The predicted values of HIA were all greater than 98%, indicating that these compounds could be smoothly absorbed into the small intestine after oral administration. In the prediction model of Caco-2, **19J** and **19P** exhibited poor results, while other compounds had a predicted value greater than 50%. The Ames test was designed to predict the mutagenic properties of compounds. As can be seen, all compounds had no mutagenic ability and were not classified as potential genotoxic substances. LD₅₀ values in the acute toxicity program of rats were all very high (2.65-2.93 mol/kg), indicating that the toxicity of the compounds was low and had a large safety window. According to the above prediction results, we selected the representative compound **19n** to carry out the relevant *in vivo* studies.

Table 3. ADMET parameter prediction of partial compounds

Compd.	BBB penetration		HIA (%)	Caco-2 permeability	AMES mutagenesis	Rat acute toxicity
	CNS activity	%				LD ₅₀ (mol/kg)
19h	+	89	98	+	-	2.80
19j	+	90	98	-	-	2.75
19k	+	93	99	+	-	2.81

19l	+	94	99	+	-	2.65
19m	+	93	99	+	-	2.70
19n	+	94	99	+	-	2.93
19p	+	94	99	-	-	2.90
20b	+	92	99	+	-	2.81
20d	+	92	99	+	-	2.81
20f	+	90	99	+	-	2.80
20i	+	90	99	+	-	2.77
20l	+	90	99	+	-	2.73
20n	+	92	99	+	-	2.90
20p	+	92	99	+	-	2.90

"+" means predicted value greater than 50%, "-" means no significant effect

2.14 Acute Toxicity Studies

The acute toxicity profiles of compound **19n** and control donepezil were evaluated in adult ICR mice (8-10 weeks old, female). The test compound **19n** was given in single doses of 1200 mg/kg by intragastric infusion (n = 20) and donepezil was given in single doses of 21.30, 26.62, 33.28, 41.6, or 52.00 mg/kg by intragastric infusion (n = 8 for each dosage). Any abnormal behavior and mortality changes were observed continuously for the first 4 hours after the compounds were administered, intermittently for the next 24 hours, and occasionally thereafter for 14 days for any delayed effects. Acute toxicity phenomena such as mortality, significant abnormal behaviors, drastically altered water or food consumption, and marked weight loss or gain were not observed during the observation period for compound **19n**. on the contrary, after oral administration of donepezil, mice in each dose group showed decreased activity, listlessness, paralysis and death, and the higher the dose, the more obvious symptoms, the shorter the time of death. The LD₅₀ of donepezil was 28.124 ± 4.631 mg/kg. Overall, these results revealed that compound **19n** was well tolerated and exhibited no acute toxicity at a dose up to 1200 mg/kg.

2.15 **19n** ameliorated scopolamine-induced cognitive impairment in mice

The learning and memory assessments were performed using the Morris water maze model by administering compound **19n** to the scopolamine-induced AD mice, which suffer from learning and memory dysfunction, with donepezil as the positive control. Thirty-two female ICR mice were randomly allocated into 4 groups (n = 8 for each group): control, model, compound **19n** (15 mg/kg/day), and donepezil (5 mg/kg/day). The experiment lasted for 16 days, with mice first undergoing a 10-day modeling period, then another 5 days of training in a water maze. On the 16th day, behavioral performance was evaluated using the Morris water maze task, which demanded incremental learning of the location of a fixed, hidden platform throughout the training period. As shown in Table 4 and Fig. 15, there were significant differences between the model group and the control group (Latency to target 32.56 ± 15.30 vs 71.89 ± 25.59 ; 7.35 ± 3.43 vs 16.93 ± 5.88), indicating that this mice model was successfully established. The latency of the target for the mice that were administered donepezil (37.88 ± 32.10 , $p < 0.05$) and compound **19n** (35.22 ± 27.53 , $p < 0.05$) were remarkably improved compared to the model group (71.89 ± 25.59) (Fig. 15E). Meanwhile, the mice treated with donepezil (7.95 ± 7.07 , $p < 0.05$) and **19n** (8.05 ± 6.12 , $p < 0.05$) spent less distance to the target compared to the model group (16.93 ± 5.88) (Fig. 15F). Taken together, these overall behavioral performance observations and results demonstrated that compound **19n** can markedly improve the learning and memory of the scopolamine-induced AD mice.

Table 4. Effects of **19n** (15 mg/kg) on scopolamine-induced memory impairment in ICR mice evaluated by the Morris water maze test*.

Group	Latency to target (s)	Distance to target (m)
control	32.56 ± 15.30	7.35 ± 3.43
model	$71.89 \pm 25.59^{##}$	$16.93 \pm 5.88^{##}$
19n	$35.22 \pm 27.53^*$	$8.05 \pm 6.12^*$
donepezil	$37.88 \pm 32.10^*$	$7.95 \pm 7.07^*$

*Donepezil (5 mg/kg) was used as the reference drug. Data were presented as the mean \pm SEM (n = 8; #p < 0.05, ##p < 0.01, control group vs. scopolamine model group; *p < 0.05, **p < 0.01, 19n or donepezil group vs. scopolamine model group).

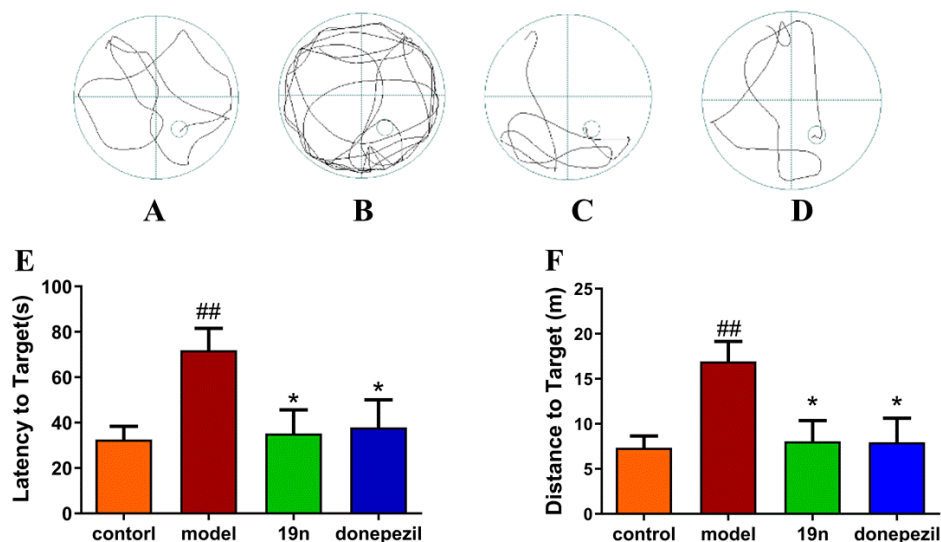


Fig. 15. Anti-AD effects of intraperitoneal injection of **19n** (15 mg/kg), donepezil (5 mg/kg) on scopolamine-induced cognitive impairment in ICR mice were determined by the Morris water maze test. The trajectories of mice were shown as the (A) control, (B) model, (C) **19n**, (D) donepezil groups, (E) The latency to target, (F) The distance to the target. Data were presented as the mean \pm SEM (n = 8; #p < 0.05, ##p < 0.01, Control group vs. scopolamine model group; *p < 0.05, **p < 0.01, **19n** or donepezil group vs. scopolamine model group).

2.16 **19n** ameliorated oligomerized $A\beta_{1-42}$ -induced cognitive impairment in mice.

To evaluate whether **19n** could overcome the oligomerized $A\beta_{1-42}$ -induced cognitive impairment, we performed the Morris water maze and Y-maze tests. Sixty male C57bl/6 mice were randomly allocated into 4 groups (n = 15 for each group): control, model, compound **19n** (15 mg/kg/day) and donepezil (5 mg/kg/day). The experiment lasted for 10 days, with mice first undergoing a 3-day modeling period, then another 5 days of training in a water maze, followed by a Y-maze test on the tenth day. On the 9th day, behavioral performance was evaluated using the Morris water maze

task. As shown in Fig. 16B, $A\beta_{1-42}$ treatment mice notably increased escape latency compared to the corresponding controls ($***P < 0.001$; Fig. 16B). Interestingly, treatment with **19n** significantly decreased escape latency compared to the Veh+ $A\beta_{1-42}$ group ($##p < 0.01$; Fig. 16B) and treatment with donepezil does not significantly decrease escape latency compared to the Veh + $A\beta_{1-42}$ group. In addition, the mice in the Veh + $A\beta_{1-42}$ group displayed a significant decrease in the percentage of time spent in the target quadrant and the ratio of brain weight to the body weight compared to the controls, suggesting memory impairment in the $A\beta_{1-42}$ -treated mice. However, mice in the $A\beta_{1-42}$ + **19n** group and $A\beta_{1-42}$ + donepezil group showed significant increases in both times spent in the target quadrant and the ratio of brain weight to the bodyweight compared to the Veh + $A\beta_{1-42}$ group (Fig. 16C and D). On the ninth day of the trial, the Y-maze test was performed to evaluate the effect of compound **19n**, and spontaneous alternations were calculated, which is a measure of spatial working memory. The % spontaneous alternations were significantly reduced in the Veh + $A\beta_{1-42}$ group of animals (Fig. 16E, $p < 0.01$) compared to the controller indicative of induction of memory and learning impairment. $A\beta_{1-42}$ + **19n** and $A\beta_{1-42}$ + donepezil groups showed significantly increased duration in the novel arm (Fig. 16E) compared to the Veh + $A\beta_{1-42}$ group. The overall results suggested that the potential of **19n** ameliorates $A\beta_{1-42}$ -induced cognitive impairment in mice.

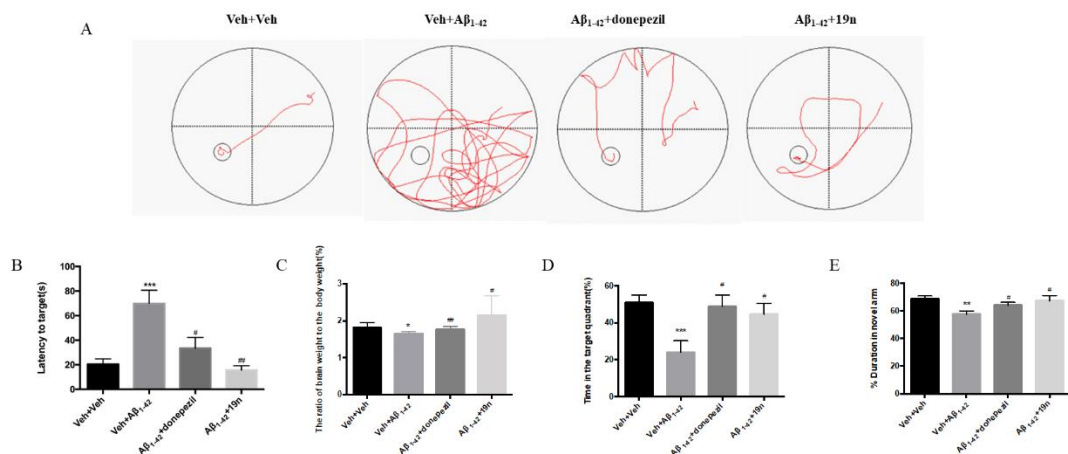


Fig. 16. Anti-AD effects of intragastric administration of **19n** (15 mg/kg), donepezil (5 mg/kg) on $A\beta_{1-42}$ -induced cognitive impairment in C57bl/6 mice determined by the Morris water maze and Y-maze test. (A) The mice were shown as the control, model,

donepezil, and **19n** groups (n=15). (B) The escape latency to target, (C) The ratio of brain weight to the body weight, (D) The time in the target quadrant, (E) The duration in novel arm. Data were presented as the mean \pm SEM (n = 15; *p < 0.05, **p < 0.01, ***p < 0.001, Control group vs. A β_{1-42} model group; #p < 0.05, ##p < 0.01, ###p < 0.001, **19n** or donepezil group vs. A β_{1-42} model group).

2.17 Compound **19n** decreased the levels of proinflammatory cytokines induced by A β_{1-42} in mice.

Inflammatory mediators play important roles in cognitive dysfunction. To determine the effect of **19n** on A β_{1-42} -induced proinflammatory cytokine production, we examined the abundance of interleukin-1 β (IL-1 β) and tumor necrosis factor- α (TNF- α) in the cortex by the ELISA assay. In A β_{1-42} -treated mice, increased levels of IL-1 β and TNF- α were observed in the cortex, while **19n** or donepezil treatment largely reduced their levels in the cortex (Fig. 17 A and B).

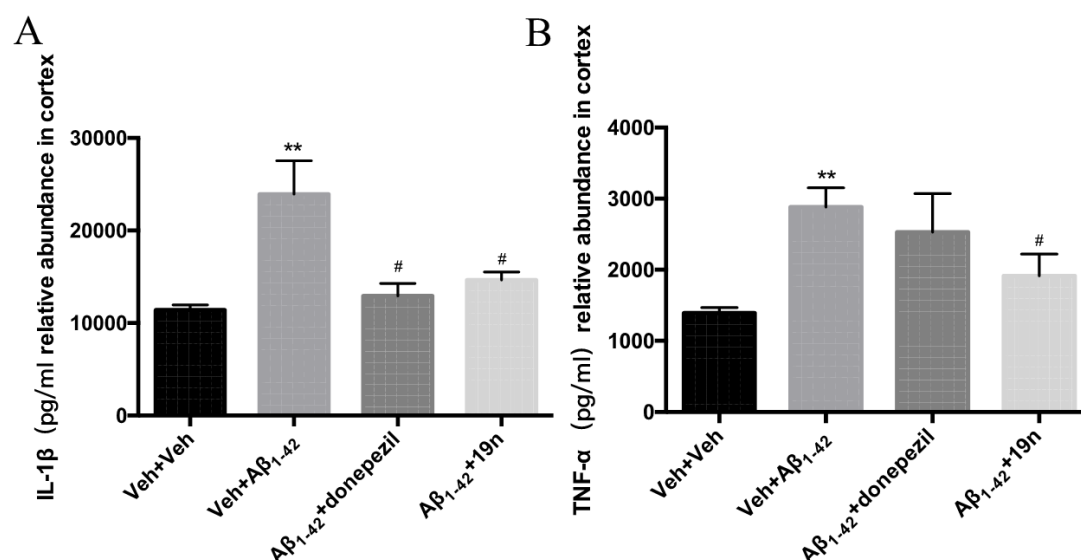


Fig. 17. The abundance of relative proinflammatory cytokine in the cortex. (A) The abundance of IL-1 β in the cortex. (B) The abundance of TNF- α in the cortex.

3. Conclusions

Accumulated evidences show that the etiology of AD is multifaceted, and each pathogenesis pathway interacts with each other [39-42]. It is difficult to control or cure the disease effectively with single target therapeutics. The current work presents the design, synthesis, and biological evaluation of a series of novel MTDLs by fusing the pharmacophores of a potent donepezil derivative with clioquinol. Most of the target compounds exhibit moderate to potent AChE inhibitory activities, the AChE IC₅₀ of the optimal compound **19n** is 0.11 ± 0.10 μ M. In addition, **19n** shows a potent copper-chelating ability with chelating dose ratio at 1:1, strong modulations of both metal-induced and AChE-induced A β aggregation, and no toxicity on SH-SY5Y cells observed at a concentration up to 50 μ M. Molecular docking and kinetic study reveal that **19n** can bind to both CAS and PAS active sites of AChE. Moreover, compound **19n** demonstrates its neuroprotection against okadaic acid-induced damage to mitochondrial functions and oxidative stress. Importantly, **19n** was well tolerated *in vivo* (>1200 mg/kg) than the positive donepezil. Furthermore, *in vivo* animal studies revealed that **19n** significantly ameliorates the cognition impairment in scopolamine-induced and oligomerized A β ₁₋₄₂ induced mouse models. Finally, it was found that **19n** significantly decreases the production of proinflammatory cytokines induced by oligomerized A β ₁₋₄₂. In summary, all the results suggest that **19n** is a promising multifunctional lead to be further developed as a potential novel MTDLs for AD treatment.

4. Experimental section

4.1 Chemistry

4.1.1 General methods

All starting materials and reference compounds were obtained from commercial sources without further purification. The ¹H NMR and ¹³C NMR spectra were recorded on a Bruker BioSpin GmbH spectrometer (Bruker, Germany) at 300 and 75 MHz respectively, where CDCl₃, MeOD, or DMSO-*d*₆ were used as the solvent. Tetramethylsilane was used as the standard and chemical shifts are reported in parts per million (ppm), coupling constants *J* are given in Hertz (Hz), and spin multiplicities are

given as singlet (s), broad singlet (brs), doublet (d), doublet of doublets (dd), triplet (t), and multiplet (m). The mass spectrometry (MS, HRMS) data of the compounds were measured using Agilent 1100-LC-MSD-Trap/SL or FTMS-2000 mass spectrometer. The reagents are all commercially available chemically pure or analytical pure products. Dry acetonitrile (MeCN) is treated with anhydrous magnesium sulfate and left to stand overnight; anhydrous methanol (MeOH) and anhydrous ethanol (EtOH) are directly used as a commercially available anhydrous solvent; commercially available acetic anhydride reagent with opening or opening soon. HCl EA solution is prepared by passing the HCl gas produced by mixing concentrated sulfuric acid and solid sodium chloride into the cold EA solution; other solvents are not treated unless otherwise specified use directly. All the reactions were routinely monitored by thin-layer chromatography on silica gel and visualized using UV light (254 nm light source). The purity ($\geq 95\%$) of compound **19n** was determined by HPLC, eluted with MeOH/0.2 mol/L ammonium acetate = 90/10, at a flow rate of 1 mL/min.

4.1.2 General procedure for the preparation of compounds 11 and 12

To a stirred solution of compounds **9** or **10** (31.41 mmol) in acetic anhydride (60 mL), 4-pyridineformaldehyde (32.98 mmol) was added under Ar atmosphere. The reaction mixture was stirred at 60°C for 10 h. After the completion of the reaction, the mixture was cooled to room temperature. Water (100 mL) was added and slowly add saturated sodium bicarbonate solution to adjust the pH of the solution to neutral, the mixture was extracted three times with ethyl acetate (50 mL \times 3), washed with cool water and saturated brine. The combined organic layer was dried in anhydrous sodium sulfate, filtered, and concentrated. The crude product was purified by flash column chromatography using 50% ethyl acetate in petroleum ether to yield pure products **11** and **12** as a yellow solid.

4.1.3 (E)-2-(2-(pyridin-4-yl)vinyl)quinolin-8-yl acetate (11)

Yellow solid, yield: 32.9%, ^1H NMR (300 MHz, CDCl_3) δ 8.68 (d, $J = 5.6$ Hz, 2H), 8.21 (d, $J = 8.6$ Hz, 1H), 7.74 (d, $J = 8.0$ Hz, 1H), 7.71 - 7.65 (m, 1H), 7.59 (d, $J = 7.9$ Hz, 1H), 7.56 (d, $J = 2.4$ Hz, 1H), 7.54 - 7.46 (m, 4H), 2.61 (s, 3H). ^{13}C NMR (75 MHz, CDCl_3) δ 164.5, 156.7, 149.2, 149.2, 147.9, 144.1, 140.5, 139.0, 136.4, 130.7, 128.3, 126.6, 123.2, 123.2, 122.8, 121.7, 119.0, 20.6. MS (ESI) m/z : 291.15 $[\text{M}+\text{H}]^+$.

4.1.4 General procedure for the preparation of compounds **13a-p** and **14a-p**

To a stirred solution of compounds **11** or **12** (0.69 mmol) in anhydrous acetonitrile (10 mL), substituted benzyl bromide (3.44 mmol) was added. The mixture was refluxed for five hours. After the completion of the reaction, the mixture was cooled to room temperature and concentrated. Ethyl acetate (10 mL) was added and the mixture was stirred for 30 minutes, filtered and dry to afford the compounds **13a-p** and **14a-p**.

4.1.5 (*E*)-4-(2-(8-acetoxyquinolin-2-yl)vinyl)-1-benzylpyridin-1-ium (**13a**)

Red solid, yield: 85.6%, ^1H NMR (300 MHz, $\text{DMSO}-d_6$) δ 9.22 (d, $J = 6.6$ Hz, 2H), 8.56 (d, $J = 8.6$ Hz, 1H), 8.48 (d, $J = 6.6$ Hz, 2H), 8.14 (d, $J = 16.3$ Hz, 1H), 8.01 (d, $J = 8.3$ Hz, 1H), 7.93 (d, $J = 7.1$ Hz, 1H), 7.65 (t, $J = 7.7$ Hz, 1H), 7.61 - 7.54 (m, 3H), 7.48 (d, $J = 5.2$ Hz, 1H), 7.45 (s, 2H), 5.85 (s, 2H), 2.52 (s, 3H). ^{13}C NMR (75 MHz, $\text{DMSO}-d_6$) δ 164.5, 157.2, 157.0, 147.8, 146.3, 146.3, 140.8, 140.1, 136.5, 134.9, 130.1, 129.4, 129.4, 129.0, 128.3, 128.3, 126.7, 125.4, 124.0, 124.0, 122.9, 121.7, 120.0, 61.8, 20.5. MS (ESI) m/z : 381.52 $[\text{M}]^+$.

4.1.6 General procedure for the preparation of compounds **17a-p** and **18a-p**

To a stirred solution of compounds **13a-p** or **14a-p** (0.84 mmol) in anhydrous ethanol (10 mL) at 0°C , sodium borohydride (1.68 mmol) was added. The reaction mixture was stirred at 0°C for 1 h. After the completion of the reaction, the reaction solution was warmed gradually to room temperature, and the reaction was quenched with saturated solution of ammonium chloride. The product was extracted with ethyl acetate three times, washed with cool water and saturated brine. The combined organic layer was dried in sodium sulfate, filtered, and concentrated to afford **15a-p** or **16a-p**.

To a mixture of compounds **15a-p** or **16a-p** (0.84 mmol) in anhydrous methanol (10 mL), anhydrous potassium carbonate (1.68 mmol) was added. The reaction mass was stirred at the same temperature for 30 minutes. After the completion of the reaction, the mixture was concentrated and extracted three times with ethyl acetate (10 mL \times 3), washed with cool water and saturated brine. The combined organic layer was dried in anhydrous sodium sulfate, filtered, and concentrated. The crude product was purified by flash column chromatography using 20% ethyl acetate in petroleum ether to yield pure products **17a-p** and **18a-p** as a yellow oil.

4.1.7 *(E)*-2-(2-(1-benzyl-1,2,3,6-tetrahydropyridin-4-yl)vinyl)quinolin-8-ol (**17a**)

Yellow oil, yield: 25.8%. ^1H NMR (300 MHz, CDCl_3) δ 8.09 (d, $J = 8.6$ Hz, 1H), 7.57 (d, $J = 8.6$ Hz, 1H), 7.44 (t, $J = 6.1$ Hz, 4H), 7.41 (s, 1H), 7.39 (t, $J = 3.0$ Hz, 1H), 7.36 (dd, $J = 5.9, 2.7$ Hz, 1H), 7.33 - 7.28 (m, 1H), 7.23 - 7.17 (m, 1H), 6.74 (d, $J = 16.1$ Hz, 1H), 6.08 (s, 1H), 3.71 (s, 2H), 3.25 (s, 2H), 2.78 (t, $J = 5.7$ Hz, 2H), 2.55 (s, 2H). ^{13}C NMR (75 MHz, CDCl_3) δ 153.5, 153.1, 140.9, 138.7, 137.3, 136.5, 133.8, 129.3, 128.6, 128.6, 128.1, 128.1, 127.7, 126.3, 125.5, 123.9, 121.4, 117.0, 112.9, 64.5, 52.3, 49.7, 27.1. MS (ESI) m/z : 343.25 $[\text{M}+\text{H}]^+$.

4.1.8 General procedure for the preparation of target compounds **19a-p** and **20a-p**

To a stirred solution of compounds **17a-p** or **18a-p** (0.52 mmol) in ethyl acetate (5 mL) at 0°C, Saturated hydrogen chloride in ethyl acetate was added dropwise at 0°C. After the completion of the reaction, the mixture was warmed to room temperature. The mixture was concentrated and recrystallized with dichloromethane-petroleum ether to afford the target compounds **19a-p** and **20a-p**.

4.1.9 *(E)*-2-(2-(1-benzyl-1,2,3,6-tetrahydropyridin-4-yl)vinyl)quinolin-8-ol hydrochloride (**19a**)

Green solid, yield: 50.1%. ^1H NMR (300 MHz, MeOD) δ 8.94 (d, $J = 8.9$ Hz, 1H), 8.42 (d, $J = 9.0$ Hz, 1H), 7.94 (d, $J = 16.1$ Hz, 1H), 7.80 - 7.70 (m, 1H), 7.70 - 7.63 (m, 2H), 7.61 - 7.54 (m, 3H), 7.46 (d, $J = 7.0$ Hz, 1H), 7.35 (d, $J = 16.1$ Hz, 1H), 6.46 (s,

1H), 4.55 (s, 2H), 4.05 (s, 2H), 3.87 (brs, 1H), 3.48 (brs, 1H), 2.94 (s, 2H). ¹³C NMR (75 MHz, DMSO-*d*₆) δ 151.7, 147.9, 145.3, 143.6, 133.7, 131.1, 131.1, 130.2, 130.0, 129.5, 129.1, 129.1, 128.8, 128.7, 128.4, 119.0, 118.6, 118.4, 116.3, 59.5, 50.1, 48.6, 21.7. HR-MS (ESI) *m/z*: calcd for C₂₃H₂₃N₂O [M+H]⁺ 343.1805, found 343.1809.

4.1.10 (E)-2-(2-(1-(2-fluorobenzyl)-1,2,3,6-tetrahydropyridin-4-yl)vinyl)quinolin-8-ol hydrochloride (19b)

Yellow solid, yield: 51.4%. ¹H NMR (300 MHz, MeOD) δ 8.97 (d, *J* = 8.8 Hz, 1H), 8.46 (d, *J* = 8.9 Hz, 1H), 7.97 (d, *J* = 16.1 Hz, 1H), 7.75 (q, *J* = 8.2 Hz, 3H), 7.64 (dd, *J* = 13.0, 6.8 Hz, 1H), 7.48 (d, *J* = 7.1 Hz, 1H), 7.38 (dd, *J* = 21.9, 7.8 Hz, 3H), 6.50 (s, 1H), 4.65 (s, 2H), 4.13 (s, 2H), 3.91 (brs, 1H), 3.53 (brs, 1H), 2.95 (s, 2H). ¹³C NMR (75 MHz, DMSO-*d*₆) δ 163.3, 160.0, 151.6, 148.0, 145.5, 143.7, 133.6, 132.9, 130.5, 129.3, 128.7, 128.4, 125.2, 119.0, 118.6, 116.7, 116.1, 115.9, 115.7, 57.4, 52.5, 50.1, 21.8. HR-MS (ESI) *m/z*: calcd for C₂₃H₂₂FN₂O [M+H]⁺ 361.1711, found 361.1708.

4.1.11 (E)-2-(2-(1-(3-fluorobenzyl)-1,2,3,6-tetrahydropyridin-4-yl)vinyl)quinolin-8-ol hydrochloride (19c)

Yellow solid, yield: 52.6%. ¹H NMR (300 MHz, MeOD) δ 8.97 (d, *J* = 8.8 Hz, 1H), 8.45 (d, *J* = 8.9 Hz, 1H), 7.96 (d, *J* = 16.1 Hz, 1H), 7.75 (q, *J* = 8.3 Hz, 2H), 7.66 - 7.55 (m, 1H), 7.56 - 7.44 (m, 3H), 7.35 (dd, *J* = 17.4, 12.2 Hz, 2H), 6.48 (s, 1H), 4.58 (d, *J* = 9.1 Hz, 2H), 4.10 (d, *J* = 17.9 Hz, 2H), 3.88 (brs, 1H), 3.43 (brs, 1H), 2.95 (s, 2H). ¹³C NMR (75 MHz, DMSO-*d*₆) δ 164.3, 161.1, 152.2, 148.5, 145.0, 143.2, 134.0, 132.2, 131.4, 130.3, 129.9, 128.9, 127.9, 120.3, 119.0, 118.7, 118.4, 117.2, 116.6, 58.3, 50.6, 50.2, 21.9. HR-MS (ESI) *m/z*: calcd for C₂₃H₂₂FN₂O [M+H]⁺ 361.1711, found 361.1711.

4.1.12 (E)-2-(2-(1-(4-fluorobenzyl)-1,2,3,6-tetrahydropyridin-4-yl)vinyl)quinolin-8-ol hydrochloride (19d)

Yellow solid, yield: 55.1%. ¹H NMR (300 MHz, MeOD) δ 8.96 (d, *J* = 8.8 Hz, 1H), 8.45 (d, *J* = 8.8 Hz, 1H), 7.96 (d, *J* = 16.1 Hz, 1H), 7.83 - 7.64 (m, 4H), 7.47 (dd, *J* =

7.0, 1.6 Hz, 1H), 7.42 - 7.24 (m, 3H), 6.48 (s, 1H), 4.56 (d, $J = 7.3$ Hz, 2H), 4.09 (d, $J = 21.8$ Hz, 2H), 3.87 (brs, 1H), 3.47 (brs, 1H), 2.94 (s, 2H). ^{13}C NMR (75 MHz, DMSO- d_6) δ 165.8, 162.5, 152.8, 149.2, 145.5, 144.0, 135.0, 134.9, 134.7, 130.9, 130.7, 129.4, 126.8, 120.9, 119.7, 119.6, 117.2, 116.9, 116.6, 58.7, 50.5, 49.6, 22.5. HR-MS (ESI) m/z : calcd for $\text{C}_{23}\text{H}_{22}\text{FN}_2\text{O}$ $[\text{M}+\text{H}]^+$ 361.1711, found 361.1715.

4.1.13 *(E)-2-(2-(1-(2-chlorobenzyl)-1,2,3,6-tetrahydropyridin-4-yl)vinyl)quinolin-8-ol hydrochloride (19e)*

Brown solid, yield: 58.2%. ^1H NMR (400 MHz, MeOD) δ 8.95 (d, $J = 8.9$ Hz, 1H), 8.42 (t, $J = 13.4$ Hz, 1H), 7.95 (d, $J = 16.2$ Hz, 1H), 7.83 (dt, $J = 12.5, 6.2$ Hz, 1H), 7.78 - 7.68 (m, 2H), 7.64 (dd, $J = 7.8, 1.3$ Hz, 1H), 7.61 - 7.47 (m, 2H), 7.46 (dd, $J = 7.3, 1.4$ Hz, 1H), 7.36 (d, $J = 16.2$ Hz, 1H), 6.48 (s, 1H), 4.67 (d, $J = 42.4$ Hz, 2H), 4.16 (s, 2H), 3.85 (brs, 1H), 3.67 (brs, 1H), 2.94 (s, 2H). ^{13}C NMR (75 MHz, DMSO- d_6) δ 151.5, 148.0, 145.4, 143.6, 135.6, 133.7, 133.6, 132.0, 130.5, 130.2, 129.2, 128.7, 128.4, 128.0, 126.7, 119.0, 118.6, 118.4, 116.7, 56.0, 50.3, 31.4, 22.4. HR-MS (ESI) m/z : calcd for $\text{C}_{23}\text{H}_{22}\text{ClN}_2\text{O}$ $[\text{M}+\text{H}]^+$ 377.1415, found 377.1408.

4.1.14 *(E)-2-(2-(1-(3-chlorobenzyl)-1,2,3,6-tetrahydropyridin-4-yl)vinyl)quinolin-8-ol hydrochloride (19f)*

Yellow solid, yield: 59.0%. ^1H NMR (400 MHz, MeOD) δ 8.94 (d, $J = 8.9$ Hz, 1H), 8.42 (d, $J = 8.9$ Hz, 1H), 7.93 (d, $J = 16.1$ Hz, 1H), 7.79 - 7.65 (m, 3H), 7.57 (ddd, $J = 17.6, 14.5, 7.5$ Hz, 3H), 7.50 - 7.41 (m, 1H), 7.40 - 7.29 (m, 1H), 6.45 (s, 1H), 4.54 (d, $J = 14.7$ Hz, 2H), 4.15 - 3.93 (m, 2H), 3.85 (brs, 1H), 3.46 (brs, 1H), 2.92 (s, 2H). ^{13}C NMR (75 MHz, DMSO- d_6) δ 151.3, 147.6, 144.2, 142.4, 133.5, 133.1, 131.1, 130.7, 130.2, 129.4, 129.4, 129.2, 129.0, 128.0, 128.0, 119.4, 118.1, 118.1, 115.7, 57.5, 49.4, 47.4, 21.1. HR-MS (ESI) m/z : calcd for $\text{C}_{23}\text{H}_{22}\text{ClN}_2\text{O}$ $[\text{M}+\text{H}]^+$ 377.1415, found 377.1415.

4.1.15 *(E)-2-(2-(1-(4-chlorobenzyl)-1,2,3,6-tetrahydropyridin-4-yl)vinyl)quinolin-8-ol hydrochloride (19g)*

Yellow solid, yield: 51.6%. ^1H NMR (400 MHz, MeOD) δ 8.94 (d, J = 8.8 Hz, 1H), 8.43 (d, J = 8.9 Hz, 1H), 7.93 (d, J = 16.1 Hz, 1H), 7.78 - 7.63 (m, 4H), 7.55 (d, J = 8.1 Hz, 2H), 7.44 (dd, J = 8.1, 6.9 Hz, 1H), 7.35 (d, J = 16.0 Hz, 1H), 6.46 (s, 1H), 4.54 (q, J = 12.6 Hz, 2H), 4.12 - 3.96 (m, 2H), 3.85 (brs, 1H), 3.45 (brs, 1H), 2.92 (s, 2H). ^{13}C NMR (75 MHz, DMSO- d_6) δ 151.3, 147.4, 144.4, 142.6, 134.8, 133.1, 132.6, 132.6, 129.5, 129.1, 128.4, 128.4, 128.0, 127.7, 127.6, 119.0, 118.1, 117.9, 115.8, 57.4, 49.3, 47.2, 21.0. HR-MS (ESI) m/z : calcd for $\text{C}_{23}\text{H}_{22}\text{ClN}_2\text{O}$ $[\text{M}+\text{H}]^+$ 377.1415, found 377.1415.

4.1.16 *(E)*-2-(2-(1-(2-bromobenzyl)-1,2,3,6-tetrahydropyridin-4-yl)vinyl)quinolin-8-ol hydrochloride (**19h**)

Yellow solid, yield: 52.3%. ^1H NMR (300 MHz, MeOD) δ 8.99 (d, J = 8.8 Hz, 1H), 8.48 (d, J = 8.9 Hz, 1H), 7.99 (d, J = 16.1 Hz, 1H), 7.88 (dd, J = 12.3, 7.7 Hz, 2H), 7.77 (q, J = 8.3 Hz, 2H), 7.61 (t, J = 7.2 Hz, 1H), 7.50 (dd, J = 11.3, 4.4 Hz, 2H), 7.41 (d, J = 16.0 Hz, 1H), 6.53 (s, 1H), 4.78 (s, 2H), 4.22 (s, 2H), 3.92 (brs, 1H), 3.69 (brs, 1H), 2.99 (s, 2H). ^{13}C NMR (75 MHz, DMSO- d_6) δ 151.3, 147.4, 144.4, 142.7, 133.2, 133.1, 132.9, 131.5, 129.5, 129.1, 128.7, 128.0, 127.9, 127.8, 125.3, 119.1, 118.1, 118.0, 115.8, 57.4, 49.7, 47.5, 20.9. HR-MS (ESI) m/z : calcd for $\text{C}_{23}\text{H}_{22}\text{BrN}_2\text{O}$ $[\text{M}+\text{H}]^+$ 421.0910, found 421.0903.

4.1.17 *(E)*-2-(2-(1-(3-bromobenzyl)-1,2,3,6-tetrahydropyridin-4-yl)vinyl)quinolin-8-ol hydrochloride (**19i**)

Brown solid, yield: 53.5%. ^1H NMR (300 MHz, MeOD) δ 8.96 (d, J = 8.9 Hz, 1H), 8.44 (d, J = 8.9 Hz, 1H), 7.95 (d, J = 16.8 Hz, 2H), 7.81 - 7.63 (m, 4H), 7.58 - 7.43 (m, 2H), 7.37 (d, J = 16.1 Hz, 1H), 6.47 (s, 1H), 4.58 (t, J = 12.0 Hz, 2H), 4.06 (s, 2H), 3.87 (brs, 1H), 3.48 (brs, 1H), 2.94 (s, 2H). ^{13}C NMR (75 MHz, DMSO- d_6) δ 151.3, 147.4, 144.3, 142.5, 133.5, 133.1, 132.3, 131.3, 130.3, 129.8, 129.4, 128.9, 128.0, 127.9, 121.8, 119.1, 118.1, 117.9, 115.7, 57.4, 49.4, 47.4, 21.0. HR-MS (ESI) m/z : calcd for $\text{C}_{23}\text{H}_{22}\text{BrN}_2\text{O}$ $[\text{M}+\text{H}]^+$ 421.0910, found 421.0906.

4.1.18 (*E*)-2-(2-(1-(4-bromobenzyl)-1,2,3,6-tetrahydropyridin-4-yl)vinyl)quinolin-8-ol hydrochloride (**19j**)

Yellow solid, yield: 54.2%. ¹H NMR (300 MHz, MeOD) δ 8.96 (d, *J* = 8.8 Hz, 1H), 8.44 (d, *J* = 8.9 Hz, 1H), 7.95 (d, *J* = 16.1 Hz, 1H), 7.81 - 7.68 (m, 4H), 7.61 (d, *J* = 8.2 Hz, 2H), 7.52 - 7.43 (m, 1H), 7.37 (d, *J* = 16.1 Hz, 1H), 6.47 (s, 1H), 4.54 (d, *J* = 8.2 Hz, 2H), 4.05 (s, 2H), 3.86 (brs, 1H), 3.46 (brs, 1H), 2.94 (s, 2H). ¹³C NMR (75 MHz, DMSO-*d*₆) δ 151.3, 147.4, 144.4, 142.6, 133.1, 132.9, 132.9, 131.4, 131.4, 129.5, 129.1, 128.0, 128.0, 127.7, 123.2, 119.1, 118.1, 117.9, 115.8, 57.5, 49.3, 47.2, 21.0. HR-MS (ESI) *m/z*: calcd for C₂₃H₂₂BrN₂O [M+H]⁺ 421.0910, found 421.0902.

4.1.19 (*E*)-2-(2-(1-(2-methylbenzyl)-1,2,3,6-tetrahydropyridin-4-yl)vinyl)quinolin-8-ol hydrochloride (**19k**)

Yellow solid, yield: 57.6%. ¹H NMR (300 MHz, MeOD) δ 8.96 (d, *J* = 8.9 Hz, 1H), 8.45 (d, *J* = 8.9 Hz, 1H), 7.96 (d, *J* = 16.1 Hz, 1H), 7.81 - 7.67 (m, 2H), 7.64 (d, *J* = 7.2 Hz, 1H), 7.47 (d, *J* = 7.3 Hz, 1H), 7.44 - 7.30 (m, 4H), 6.49 (s, 1H), 4.60 (s, 2H), 4.13 (s, 2H), 3.86 (brs, 1H), 3.58 (brs, 1H), 2.94 (s, 2H), 2.56 (s, 3H). ¹³C NMR (75 MHz, DMSO-*d*₆) δ 151.3, 147.4, 144.4, 142.8, 138.3, 133.2, 131.6, 130.6, 129.5, 129.4, 129.4, 128.0, 127.7, 127.4, 125.9, 118.9, 118.1, 118.0, 115.9, 55.6, 49.6, 47.2, 21.1, 18.6. HR-MS (ESI) *m/z*: calcd for C₂₄H₂₅N₂O [M+H]⁺ 357.1961, found 357.1963.

4.1.20 (*E*)-2-(2-(1-(3-methylbenzyl)-1,2,3,6-tetrahydropyridin-4-yl)vinyl)quinolin-8-ol hydrochloride (**19l**)

Yellow solid, yield: 58.3%. ¹H NMR (300 MHz, MeOD) δ 8.95 (d, *J* = 8.8 Hz, 1H), 8.44 (d, *J* = 8.9 Hz, 1H), 7.95 (d, *J* = 16.1 Hz, 1H), 7.82 - 7.66 (m, 2H), 7.54 - 7.42 (m, 4H), 7.42 - 7.29 (m, 2H), 6.47 (s, 1H), 4.50 (d, *J* = 7.5 Hz, 2H), 4.13 - 3.95 (m, 2H), 3.85 (brs, 1H), 3.45 (brs, 1H), 2.93 (s, 2H), 2.43 (s, 3H). ¹³C NMR (75 MHz, DMSO-*d*₆) δ 151.3, 147.5, 144.1, 142.4, 138.1, 133.2, 131.4, 129.9, 129.4, 129.1, 128.7, 128.3, 127.9, 127.9, 127.7, 119.2, 118.1, 118.0, 115.7, 58.3, 49.3, 21.0, 19.9, 19.9. HR-MS (ESI) *m/z*: calcd for C₂₄H₂₅N₂O [M+H]⁺ 357.1961, found 357.1961.

4.1.21 (E)-2-(2-(1-(4-methylbenzyl))-1,2,3,6-tetrahydropyridin-4-yl)vinyl)quinolin-8ol hydrochloride (**19m**)

Yellow solid, yield: 55.3%. ¹H NMR (300 MHz, MeOD) δ 8.96 (d, *J* = 8.8 Hz, 1H), 8.45 (d, *J* = 8.9 Hz, 1H), 7.95 (d, *J* = 16.2 Hz, 1H), 7.74 (q, *J* = 8.3 Hz, 2H), 7.54 (d, *J* = 7.9 Hz, 2H), 7.50 - 7.43 (m, 1H), 7.42 - 7.31 (m, 3H), 6.48 (s, 1H), 4.58 - 4.39 (m, 2H), 4.04 (s, 2H), 3.87 (brs, 1H), 3.43 (brs, 1H), 2.93 (s, 2H), 2.44 (s, 3H). ¹³C NMR (75 MHz, DMSO-*d*₆) δ 151.3, 147.3, 144.5, 142.7, 139.3, 133.1, 130.7, 130.7, 129.5, 129.2, 129.0, 129.0, 128.0, 127.6, 125.7, 118.9, 118.1, 117.9, 115.8, 58.1, 49.2, 47.1, 21.0, 19.8. HR-MS (ESI) *m/z*: calcd for C₂₄H₂₅N₂O [M+H]⁺ 357.1961, found 357.1960.

4.1.22 (E)-2-(2-(1-(2-(trifluoromethylbenzyl))-1,2,3,6-tetrahydropyridin-4-yl)vinyl)quinolin-8ol hydrochloride (**19n**)

Brown solid, yield: 51.1%. ¹H NMR (300 MHz, MeOD) δ 8.95 (d, *J* = 8.9 Hz, 1H), 8.44 (d, *J* = 9.0 Hz, 1H), 8.07 (d, *J* = 7.4 Hz, 1H), 8.00 - 7.91 (m, 2H), 7.87 (t, *J* = 7.3 Hz, 1H), 7.80 - 7.75 (m, 1H), 7.75 - 7.68 (m, 2H), 7.46 (dd, *J* = 7.1, 1.8 Hz, 1H), 7.37 (d, *J* = 16.3 Hz, 1H), 6.47 (s, 1H), 4.74 (s, 2H), 4.16 (s, 2H), 3.82 (brs, 1H), 3.60 (brs, 1H), 2.94 (s, 2H). ¹³C NMR (75 MHz, DMSO-*d*₆) δ 151.2, 147.3, 144.5, 142.6, 133.0, 132.6, 132.4, 129.8, 129.5, 128.9, 128.0, 127.7, 127.2, 126.0, 125.3, 121.6, 119.0, 118.1, 117.9, 115.8, 54.6, 50.3, 47.2, 21.0. HR-MS (ESI) *m/z*: calcd for C₂₄H₂₂F₃N₂O [M+H]⁺ 411.1678, found 411.1678. *t_R* (HPLC) = 10.818 min; purity = 97.367%.

4.1.23 (E)-2-(2-(1-(3-(trifluoromethylbenzyl))-1,2,3,6-tetrahydropyridin-4-yl)vinyl)quinolin-8ol hydrochloride (**19o**)

Yellow solid, yield: 53.9%. ¹H NMR (300 MHz, MeOD) δ 8.93 (d, *J* = 8.9 Hz, 1H), 8.41 (d, *J* = 8.9 Hz, 1H), 8.04 (s, 1H), 7.92 (dd, *J* = 27.7, 8.7 Hz, 3H), 7.82 - 7.75 (m, 1H), 7.75 - 7.65 (m, 2H), 7.44 (dd, *J* = 7.1, 1.7 Hz, 1H), 7.39 - 7.27 (m, 1H), 6.44 (s, 1H), 4.59 (d, *J* = 31.7 Hz, 2H), 4.08 (d, *J* = 16.1 Hz, 2H), 3.85 (brs, 1H), 3.52 (brs, 1H), 2.93 (s, 2H). ¹³C NMR (75 MHz, DMSO-*d*₆) δ 151.3, 147.6, 144.2, 142.4, 135.0, 133.2, 130.3, 129.9, 129.4, 129.1, 128.0, 128.0, 127.7, 126.0, 125.3, 121.7, 119.3, 118.1, 118.1,

115.7, 57.4, 49.4, 47.2, 21.1. HR-MS (ESI) m/z : calcd for $C_{24}H_{22}F_3N_2O$ $[M+H]^+$ 411.1678, found 411.1676.

4.1.24 *(E)-2-(2-(1-(4-(trifluoromethylbenzyl))-1,2,3,6-tetrahydropyridin-4-yl)vinyl)quinolin-8-ol hydrochloride (19p)*

Green solid, yield: 58.0%. 1H NMR (300 MHz, MeOD) δ 8.92 (d, $J = 8.9$ Hz, 1H), 8.40 (d, $J = 8.8$ Hz, 1H), 8.00 - 7.81 (m, 5H), 7.79 - 7.63 (m, 2H), 7.44 (dd, $J = 7.1, 1.7$ Hz, 1H), 7.34 (d, $J = 16.3$ Hz, 1H), 6.45 (s, 1H), 4.59 (d, $J = 30.6$ Hz, 2H), 4.06 (s, 2H), 3.86 (brs, 1H), 3.52 (brs, 1H), 2.93 (s, 2H). ^{13}C NMR (75 MHz, DMSO- d_6) δ 151.2, 147.4, 144.2, 142.3, 133.1, 133.0, 131.5, 131.5, 130.8, 130.4, 129.4, 128.6, 128.0, 127.9, 125.1, 125.1, 119.0, 118.0, 117.8, 115.5, 57.6, 49.5, 47.2, 21.0. HR-MS (ESI) m/z : calcd for $C_{24}H_{22}F_3N_2O$ $[M+H]^+$ 411.1678, found 411.1685.

4.1.25 *(E)-2-(2-(1-benzyl-1,2,3,6-tetrahydropyridin-4-yl)vinyl)-5,7-dichloroquinolin-8-ol hydrochloride (20a)*

Brown solid, yield: 63.2%. 1H NMR (300 MHz, MeOD) δ 8.92 (d, $J = 9.0$ Hz, 1H), 8.34 (d, $J = 9.2$ Hz, 1H), 7.99 - 7.85 (m, 2H), 7.64 (ddd, $J = 7.0, 4.8, 3.4$ Hz, 2H), 7.59 - 7.49 (m, 3H), 7.28 (d, $J = 16.2$ Hz, 1H), 6.41 (s, 1H), 4.60 - 4.45 (m, 2H), 4.02 (s, 2H), 3.85 (d, $J = 12.0$ Hz, 1H), 3.44 (dd, $J = 18.0, 9.7$ Hz, 1H), 2.90 (s, 2H). ^{13}C NMR (101 MHz, DMSO) δ 156.11, 149.07, 139.22, 138.85, 134.34, 133.56, 132.47, 129.34, 128.71, 127.50, 127.24, 125.13, 123.88, 122.35, 122.26, 119.55, 115.88, 62.14, 53.35, 49.51, 25.44. HR-MS (ESI) m/z : calcd for $C_{23}H_{21}Cl_2N_2O$ $[M+H]^+$ 411.1026, found 411.1013.

4.1.26 *(E)-5,7-dichloro-2-(2-(1-(2-fluorobenzyl)-1,2,3,6-tetrahydropyridin-4-yl)vinyl)quinolin-8-ol hydrochloride (20b)*

Brown solid, yield: 59.6%. 1H NMR (300 MHz, MeOD) δ 8.80 (d, $J = 7.9$ Hz, 1H), 8.21 (s, 1H), 7.91 (d, $J = 12.6$ Hz, 1H), 7.81 (s, 1H), 7.74 (t, $J = 7.4$ Hz, 1H), 7.64 (dd, $J = 13.2, 7.6$ Hz, 1H), 7.46 - 7.39 (m, 1H), 7.36 (t, $J = 7.1$ Hz, 1H), 7.23 (s, 1H), 6.37 (s, 1H), 4.63 (s, 2H), 4.11 (s, 2H), 3.88 (brs, 1H), 3.53 (brs, 1H), 2.93 (s, 2H). ^{13}C NMR

(101 MHz, DMSO) δ 156.10, 149.07, 139.22, 138.80, 134.29, 133.56, 132.09, 132.05, 129.69, 127.24, 125.17, 124.74, 124.71, 123.88, 122.33, 119.56, 115.88, 115.79, 115.57, 54.59, 53.09, 49.39, 25.43. HR-MS (ESI) m/z : calcd for $C_{23}H_{20}Cl_2FN_2O$ $[M+H]^+$ 429.0931, found 429.0918.

4.1.27 *(E)-5,7-dichloro-2-(2-(1-(3-fluorobenzyl)-1,2,3,6-tetrahydropyridin-4-yl)vinyl)quinolin-8-ol hydrochloride (20c)*

Brown solid, yield: 58.5%. 1H NMR (300 MHz, MeOD) δ 8.88 (d, J = 9.0 Hz, 1H), 8.28 (d, J = 9.1 Hz, 1H), 7.93 (d, J = 16.3 Hz, 1H), 7.86 (s, 1H), 7.60 (dd, J = 13.7, 8.0 Hz, 1H), 7.50 (s, 2H), 7.33 (t, J = 8.5 Hz, 1H), 7.26 (d, J = 16.4 Hz, 1H), 6.40 (s, 1H), 4.56 (d, J = 7.0 Hz, 2H), 4.05 (s, 2H), 3.86 (brs, 1H), 3.48 (brs, 1H), 2.93 (s, 2H). ^{13}C NMR (151 MHz, DMSO) δ 163.50, 161.91, 161.88, 149.58, 149.09, 139.23, 134.31, 133.64, 130.77, 127.30, 125.51, 123.94, 122.50, 119.57, 115.90, 60.17, 49.29, 48.15, 21.11. HR-MS (ESI) m/z : calcd for $C_{23}H_{20}Cl_2FN_2O$ $[M+H]^+$ 429.0931, found 429.0919.

4.1.28 *(E)-5,7-dichloro-2-(2-(1-(4-fluorobenzyl)-1,2,3,6-tetrahydropyridin-4-yl)vinyl)quinolin-8-ol hydrochloride (20d)*

Yellow solid, yield: 59.9%. 1H NMR (300 MHz, MeOD) δ 8.96 (d, J = 9.1 Hz, 1H), 8.37 (d, J = 9.1 Hz, 1H), 8.03 - 7.87 (m, 2H), 7.70 (dd, J = 8.6, 5.3 Hz, 2H), 7.32 (d, J = 6.0 Hz, 1H), 7.29 (d, J = 8.6 Hz, 2H), 6.43 (s, 1H), 4.54 (d, J = 6.7 Hz, 2H), 4.04 (s, 2H), 3.85 (brs, 1H), 3.46 (brs, 1H), 2.93 (s, 2H). ^{13}C NMR (126 MHz, DMSO) δ 164.17, 162.21, 155.46, 149.10, 139.11, 137.11, 134.32, 134.25, 134.14, 133.91, 127.56, 127.08, 126.69, 125.32, 124.09, 122.72, 119.60, 116.24, 116.07, 116.02, 57.53, 49.46, 47.91, 21.97. HR-MS (ESI) m/z : calcd for $C_{23}H_{20}Cl_2FN_2O$ $[M+H]^+$ 429.0931, found 429.0926.

4.1.29 *(E)-5,7-dichloro-2-(2-(1-(2-chlorobenzyl)-1,2,3,6-tetrahydropyridin-4-yl)vinyl)quinolin-8-ol hydrochloride (20e)*

Yellow solid, yield: 61.8%. 1H NMR (300 MHz, MeOD) δ 8.79 (d, J = 8.9 Hz, 1H), 8.15 (dd, J = 12.7, 9.2 Hz, 1H), 7.91 (d, J = 16.2 Hz, 1H), 7.81 (d, J = 10.6 Hz, 2H), 7.67 (d, J = 7.6 Hz, 1H), 7.59 (dd, J = 7.0, 5.3 Hz, 1H), 7.55 (dd, J = 10.2, 4.8 Hz, 1H),

7.20 (d, $J = 16.1$ Hz, 1H), 6.36 (s, 1H), 4.71 (d, $J = 9.0$ Hz, 2H), 4.13 (d, $J = 13.1$ Hz, 2H), 3.88 (brs, 1H), 3.59 (brs, 1H), 2.94 (s, 2H). ^{13}C NMR (75 MHz, DMSO- d_6) δ 153.7, 145.5, 139.3, 138.8, 134.7, 134.1, 133.2, 133.0, 131.3, 131.2, 129.4, 127.7, 127.1, 126.6, 123.6, 122.8, 120.1, 120.0, 118.1, 55.1, 49.7, 48.0, 21.0. HR-MS (ESI) m/z : calcd for $\text{C}_{23}\text{H}_{20}\text{Cl}_3\text{N}_2\text{O}$ $[\text{M}+\text{H}]^+$ 445.0635, found 445.0618.

4.1.30 *(E)*-5,7-dichloro-2-(2-(1-(3-chlorobenzyl)-1,2,3,6-tetrahydropyridin-4-yl)vinyl)quinolin-8-ol hydrochloride (**20f**)

Brown solid, yield: 62.7%. ^1H NMR (300 MHz, MeOD) δ 8.98 (d, $J = 9.1$ Hz, 1H), 8.40 (d, $J = 9.2$ Hz, 1H), 8.03 - 7.91 (m, 2H), 7.76 (s, 1H), 7.62 (dd, $J = 6.5, 4.6$ Hz, 1H), 7.59 (d, $J = 2.0$ Hz, 1H), 7.55 (d, $J = 7.6$ Hz, 1H), 7.33 (d, $J = 16.3$ Hz, 1H), 6.45 (s, 1H), 4.56 (d, $J = 9.5$ Hz, 2H), 4.06 (s, 2H), 3.86 (brs, 1H), 3.49 (brs, 1H), 2.94 (s, 2H). ^{13}C NMR (151 MHz, DMSO) δ 155.44, 149.14, 139.18, 136.98, 134.11, 133.90, 133.81, 132.67, 131.66, 131.16, 130.58, 130.01, 127.58, 127.20, 125.18, 124.12, 122.78, 119.60, 115.99, 57.71, 49.77, 48.26, 21.99. HR-MS (ESI) m/z : calcd for $\text{C}_{23}\text{H}_{20}\text{Cl}_3\text{N}_2\text{O}$ $[\text{M}+\text{H}]^+$ 445.0635, found 445.0620.

4.1.31 *(E)*-5,7-dichloro-2-(2-(1-(4-chlorobenzyl)-1,2,3,6-tetrahydropyridin-4-yl)vinyl)quinolin-8-ol hydrochloride (**20g**)

Brown solid, yield: 60.0%. ^1H NMR (300 MHz, MeOD) δ 8.97 (d, $J = 9.1$ Hz, 1H), 8.39 (d, $J = 9.2$ Hz, 1H), 7.97 (d, $J = 16.1$ Hz, 1H), 7.91 (s, 1H), 7.68 (d, $J = 7.2$ Hz, 1H), 7.65 (d, $J = 6.6$ Hz, 1H), 7.59 (s, 1H), 7.56 (s, 1H), 7.30 (t, $J = 12.7$ Hz, 1H), 6.45 (s, 1H), 4.55 (d, $J = 7.6$ Hz, 2H), 4.14 - 3.96 (m, 2H), 3.85 (brs, 1H), 3.45 (brs, 1H), 2.93 (s, 2H). ^{13}C NMR (126 MHz, DMSO) δ 170.00, 166.49, 161.39, 151.17, 147.36, 126.11, 121.57, 120.64, 64.36, 57.48, 52.58, 20.49. HR-MS (ESI) m/z : calcd for $\text{C}_{23}\text{H}_{20}\text{Cl}_3\text{N}_2\text{O}$ $[\text{M}+\text{H}]^+$ 445.0635, found 445.0620.

4.1.32 *(E)*-5,7-dichloro-2-(2-(1-(2-bromobenzyl)-1,2,3,6-tetrahydropyridin-4-yl)vinyl)quinolin-8-ol hydrochloride (**20h**)

Yellow solid, yield: 59.8%. ¹H NMR (400 MHz, MeOD) δ 8.74 (d, *J* = 8.9 Hz, 1H), 8.12 (dd, *J* = 11.5, 6.4 Hz, 1H), 7.88 (d, *J* = 16.2 Hz, 1H), 7.84 - 7.78 (m, 2H), 7.76 (s, 1H), 7.57 (td, *J* = 7.6, 1.1 Hz, 1H), 7.52 - 7.43 (m, 1H), 7.16 (d, *J* = 16.0 Hz, 1H), 6.34 (s, 1H), 4.70 (d, *J* = 12.4 Hz, 2H), 4.14 (s, 2H), 3.83 (brs, 1H), 3.62 (brs, 1H), 2.92 (s, 2H). ¹³C NMR (75 MHz, DMSO-*d*₆) δ 154.4, 150.2, 147.2, 134.1, 133.6, 133.3, 133.2, 132.9, 131.5, 128.8, 127.9, 127.1, 125.4, 125.3, 124.7, 123.4, 121.1, 119.4, 116.2, 57.4, 49.5, 48.6, 21.1. HR-MS (ESI) *m/z*: calcd for C₂₃H₂₀Cl₂BrN₂O [M+H]⁺ 489.0130, found 489.0117.

4.1.33 *(E)*-5,7-dichloro-2-(2-(1-(3-bromobenzyl)-1,2,3,6-tetrahydropyridin-4-yl)vinyl)quinolin-8-ol hydrochloride (**20i**)

Yellow solid, yield: 57.1%. ¹H NMR (400 MHz, MeOD) δ 8.96 (d, *J* = 8.9 Hz, 1H), 8.36 (d, *J* = 8.9 Hz, 1H), 8.00 - 7.85 (m, 3H), 7.73 (d, *J* = 8.2 Hz, 1H), 7.64 (d, *J* = 7.7 Hz, 1H), 7.48 (dd, *J* = 9.7, 6.1 Hz, 1H), 7.30 (d, *J* = 16.1 Hz, 1H), 6.41 (s, 1H), 4.52 (d, *J* = 15.6 Hz, 2H), 4.00 (d, *J* = 21.9 Hz, 2H), 3.84 (brs, 1H), 3.55 - 3.38 (m, 1H), 2.91 (s, 2H). ¹³C NMR (151 MHz, DMSO) δ 155.45, 149.13, 139.16, 137.02, 134.51, 134.10, 133.91, 132.94, 132.88, 131.38, 130.96, 127.58, 127.17, 125.21, 124.11, 122.77, 122.38, 119.61, 116.01, 57.65, 49.73, 48.25, 21.98. HR-MS (ESI) *m/z*: calcd for C₂₃H₂₀Cl₂BrN₂O [M+H]⁺ 489.0130, found 489.0110.

4.1.34 *(E)*-5,7-dichloro-2-(2-(1-(4-bromobenzyl)-1,2,3,6-tetrahydropyridin-4-yl)vinyl)quinolin-8-ol hydrochloride (**20j**)

Brown solid, yield: 53.4%. ¹H NMR (400 MHz, MeOD) δ 9.02 (d, *J* = 9.0 Hz, 1H), 8.44 (d, *J* = 8.1 Hz, 1H), 7.97 (d, *J* = 19.0 Hz, 2H), 7.71 (s, 1H), 7.71 - 7.66 (m, 1H), 7.59 (s, 1H), 7.57 (s, 1H), 7.35 (d, *J* = 15.8 Hz, 1H), 6.45 (s, 1H), 4.51 (d, *J* = 10.9 Hz, 2H), 4.03 (s, 2H), 3.84 (s, 1H), 3.40 (s, 1H), 2.91 (s, 2H). ¹³C NMR (75 MHz, DMSO-*d*₆) δ 155.3, 148.6, 138.6, 134.1, 134.0, 133.8, 132.2, 132.2, 130.7, 129.3, 128.6, 127.5, 126.9, 126.6, 124.1, 123.7, 119.7, 116.0, 110.7, 57.8, 49.8, 45.5, 21.0. HR-MS (ESI) *m/z*: calcd for C₂₃H₂₀Cl₂BrN₂O [M+H]⁺ 489.0130, found 489.0106.

4.1.35 (E)-5,7-dichloro-2-(2-(1-(2-methylbenzyl)-1,2,3,6-tetrahydropyridin-4-yl)vinyl)quinoline-8-ol hydrochloride (**20k**)

Brown solid, yield: 65.0%. ¹H NMR (400 MHz, MeOD) δ 8.87 (d, *J* = 9.0 Hz, 1H), 8.29 (d, *J* = 9.1 Hz, 1H), 7.92 (dd, *J* = 13.7, 8.8 Hz, 1H), 7.90 - 7.80 (m, 1H), 7.58 (dd, *J* = 11.8, 7.2 Hz, 1H), 7.42 (d, *J* = 6.6 Hz, 1H), 7.41 - 7.39 (m, 1H), 7.39 - 7.35 (m, 1H), 7.23 (dd, *J* = 18.2, 12.8 Hz, 1H), 6.40 (s, 1H), 4.56 (d, *J* = 12.5 Hz, 2H), 4.17 - 4.00 (m, 2H), 3.83 (dd, *J* = 14.8, 10.5 Hz, 1H), 3.53 (ddd, *J* = 9.7, 8.7, 5.0 Hz, 1H), 2.90 (s, 2H), 2.53 (s, 3H). ¹³C NMR (75 MHz, DMSO-*d*₆) δ 154.5, 147.4, 138.3, 137.2, 133.9, 133.5, 131.6, 130.6, 129.4, 127.6, 127.0, 125.9, 125.6, 123.4, 121.3, 121.3, 119.3, 116.0, 111.6, 55.5, 49.6, 48.7, 21.3, 18.7. HR-MS (ESI) *m/z*: calcd for C₂₄H₂₃Cl₂N₂O [M+H]⁺ 425.1182, found 425.1171.

4.1.36 (E)-5,7-dichloro-2-(2-(1-(3-methylbenzyl)-1,2,3,6-tetrahydropyridin-4-yl)vinyl)quinoline-8-ol hydrochloride (**20l**)

Yellow solid, yield: 66.4%. ¹H NMR (400 MHz, MeOD) δ 8.98 (d, *J* = 8.8 Hz, 1H), 8.41 (d, *J* = 9.0 Hz, 1H), 8.03 - 7.86 (m, 2H), 7.47 (s, 1H), 7.41 (dd, *J* = 13.4, 5.6 Hz, 2H), 7.35 (dd, *J* = 17.5, 10.2 Hz, 2H), 6.45 (s, 1H), 4.61 - 4.36 (m, 2H), 4.05 (d, *J* = 19.9 Hz, 2H), 3.85 (d, *J* = 10.6 Hz, 1H), 3.46 (d, *J* = 29.0 Hz, 1H), 2.91 (s, 2H), 2.42 (s, 3H). ¹³C NMR (126 MHz, DMSO) δ 155.46, 149.10, 139.12, 138.49, 137.11, 134.12, 133.92, 132.39, 130.56, 130.21, 129.18, 128.89, 127.57, 127.07, 125.36, 124.10, 122.74, 119.61, 116.03, 58.50, 49.62, 47.99, 21.96, 21.44. HR-MS (ESI) *m/z*: calcd for C₂₄H₂₃Cl₂N₂O [M+H]⁺ 425.1182, found 425.1174.

4.1.37 (E)-5,7-dichloro-2-(2-(1-(4-methylbenzyl)-1,2,3,6-tetrahydropyridin-4-yl)vinyl)quinoline-8-ol hydrochloride (**20m**)

Brown solid, yield: 63.1%. ¹H NMR (400 MHz, MeOD) δ 8.96 (d, *J* = 9.1 Hz, 1H), 8.38 (d, *J* = 9.2 Hz, 1H), 8.00 - 7.91 (m, 1H), 7.90 (s, 1H), 7.50 (t, *J* = 7.9 Hz, 2H), 7.38 - 7.35 (m, 1H), 7.33 (d, *J* = 9.7 Hz, 1H), 7.28 (dd, *J* = 11.8, 8.6 Hz, 1H), 6.43 (s, 1H), 4.56 - 4.36 (m, 2H), 3.98 (d, *J* = 20.7 Hz, 2H), 3.90 - 3.78 (m, 1H), 3.41 (dt, *J* = 12.2,

8.3 Hz, 1H), 2.88 (d, $J = 15.4$ Hz, 2H), 2.41 (d, $J = 9.8$ Hz, 3H). HR-MS (ESI) m/z : calcd for $C_{24}H_{23}Cl_2N_2O$ $[M+H]^+$ 425.1182, found 425.1169.

4.1.38 (E)-5,7-dichloro-2-(2-(1-(2-(trifluoromethyl)benzyl)-1,2,3,6-tetrahydropyridin-4-yl)vinyl)quinoline-8-ol hydrochloride (20n)

Brown solid, yield: 59.3%. 1H NMR (400 MHz, MeOD) δ 8.98 (d, $J = 9.1$ Hz, 1H), 8.40 (d, $J = 9.2$ Hz, 1H), 8.06 (d, $J = 7.7$ Hz, 1H), 8.02 - 7.90 (m, 3H), 7.87 (t, $J = 7.4$ Hz, 1H), 7.76 (t, $J = 7.7$ Hz, 1H), 7.32 (t, $J = 11.6$ Hz, 1H), 6.45 (s, 1H), 4.72 (d, $J = 11.3$ Hz, 2H), 4.13 (d, $J = 19.5$ Hz, 2H), 3.83 (brs, 1H), 3.64 (brs, 1H), 2.94 (s, 2H). ^{13}C NMR (75 MHz, DMSO- d_6) δ 154.4, 153.1, 147.3, 137.0, 136.9, 134.1, 133.3, 132.7, 132.5, 129.9, 127.5, 125.4, 123.6, 123.5, 121.2, 121.2, 119.4, 116.3, 116.2, 92.5, 54.4, 50.2, 42.9, 21.3. HR-MS (ESI) m/z : calcd for $C_{24}H_{20}Cl_2F_3N_2O$ $[M+H]^+$ 479.0899, found 479.0879.

4.1.39 (E)-5,7-dichloro-2-(2-(1-(3-(trifluoromethyl)benzyl)-1,2,3,6-tetrahydropyridin-4-yl)vinyl)quinoline-8-ol hydrochloride (20o)

Red solid, yield: 61.0%. 1H NMR (400 MHz, MeOD) δ 8.94 (d, $J = 7.5$ Hz, 1H), 8.36 (d, $J = 7.2$ Hz, 1H), 8.02 (d, $J = 13.7$ Hz, 1H), 8.00 - 7.91 (m, 2H), 7.88 (d, $J = 9.7$ Hz, 2H), 7.77 (t, $J = 7.6$ Hz, 1H), 7.37 - 7.22 (m, 1H), 6.42 (s, 1H), 4.62 (dd, $J = 29.7, 19.9$ Hz, 2H), 4.08 (dd, $J = 26.9, 10.7$ Hz, 2H), 3.86 (s, 1H), 3.50 (s, 1H), 2.92 (s, 2H). ^{13}C NMR (75 MHz, DMSO- d_6) δ 154.4, 147.5, 143.0, 137.3, 136.6, 134.9, 133.8, 133.4, 130.4, 129.8, 129.5, 129.4, 127.0, 126.0, 124.5, 123.4, 121.3, 119.3, 115.8, 114.8, 54.0, 49.4, 43.9, 21.3. HR-MS (ESI) m/z : calcd for $C_{24}H_{20}Cl_2F_3N_2O$ $[M+H]^+$ 479.0899, found 479.0890.

4.1.40 (E)-5,7-dichloro-2-(2-(1-(4-(trifluoromethyl)benzyl)-1,2,3,6-tetrahydropyridin-4-yl)vinyl)quinoline-8-ol hydrochloride (20p)

Red solid, yield: 52.0%. 1H NMR (400 MHz, MeOD) δ 8.96 (d, $J = 9.1$ Hz, 1H), 8.38 (d, $J = 9.2$ Hz, 1H), 8.00 - 7.92 (m, 1H), 7.90 (d, $J = 1.9$ Hz, 1H), 7.89 - 7.86 (m, 3H), 7.83 (d, $J = 11.5$ Hz, 1H), 7.35 - 7.26 (m, 1H), 6.44 (s, 1H), 4.60 (t, $J = 24.5$ Hz,

2H), 4.06 (dd, $J = 27.7, 17.8$ Hz, 2H), 3.86 (s, 1H), 3.53 - 3.42 (m, 1H), 2.90 (d, $J = 15.4$ Hz, 2H). ^{13}C NMR (151 MHz, DMSO) δ 172.47, 155.45, 149.12, 139.15, 137.03, 135.01, 134.10, 133.90, 132.79, 127.57, 127.15, 126.14, 126.12, 125.19, 124.11, 122.76, 119.60, 116.00, 57.69, 49.76, 48.28, 21.55. HR-MS (ESI) m/z : calcd for $\text{C}_{24}\text{H}_{20}\text{Cl}_2\text{F}_3\text{N}_2\text{O}$ $[\text{M}+\text{H}]^+$ 479.0899, found 479.0893.

4.2 Pharmacology

4.2.1 AChE activity assay *in vitro*

The AChE inhibitory ability of target compounds was tested by Ellman assay with slight modifications [35]. AChE from *Electrophorus electricus* (C3389, Sigma-Aldrich) was dissolved in 0.1 M phosphate buffer (pH 8.0) to prepare an AChE solution (2U/mL). 20 μL of phosphate buffer (pH 8.0) was first added to the 96-well plate, and then different concentrations of test compounds (20 μL), 1 mM 5'-dithiobis (2-nitrobenzoic acid) (DTNB) solution (100 μL), AChE solution (40 μL) were added in order. After the plate was incubated for 15 min at 37°C, 20 μL of acetylthiocholine iodide (1 mM) was added to the mixed solution. The absorbance of every plate was recorded at 405 nm using a microplate reader (MULTISKAN FC, Thermo Scientific) immediately. The inhibition of each compound was calculated by the following expression: $(1 - A_i/A_c) \times 100$, where A_i and A_c are the absorbance obtained for AChE in the presence and absence of the inhibitors, respectively. Each experiment was analyzed in triplicate. The IC_{50} values of all target compounds were evaluated graphically by using log concentration-percentage inhibition curves (Graph Pad Prism 8.0).

4.2.2 Kinetic characterization of AChE inhibition

Kinetic characterization of AChE was performed using the previously reported method [25]. The required experimental materials were the same as those used in the above AChE inhibition test. Three final concentrations (0 μM , 0.15 μM , 0.3 μM) of test compound **19n** (20 μL), 20 μL of acetylthiocholine iodide with different concentrations (1.5-4 mM), and 20 μL of PBS were added to 96 plates in order, and then 40 μL of AChE

was added. After incubating at 37 °C for 15 min, 100 µL of 0.1 mM DTNB was added. Kinetic characterization of the hydrolysis of ATC catalyzed by AChE was performed on 405 nm using a microplate reader (MULTISKAN FC, Thermo Scientific). The plots were evaluated using a weighted least squares analysis that assumes the variance of V was a constant percentage of the entire dataset V. In a weighted analysis, the slope of these maps corresponds to the concentration of the compound, and K_i was determined as the ratio of the retest intercept to the retest slope.

4.2.3 Molecular docking study

The protein structure of AChE (PDB ID: 4EY7) was downloaded from Protein Data Bank (<https://www.rcsb.org>). The protein preparation and receptor grid generation modules of Schrodinger software were used to refine AChE and define an active pocket for AChE, respectively. The ligand preparation module was used to refine small molecules. Finally, the ligand docking module was used to dock small molecules to AChE.

4.2.4 Metal-chelating study

The study of metal chelation was carried out by UV-Vis spectrophotometer. The absorption spectra of each compound (40 µM, final concentration) alone or in the presence of CuSO₄, FeSO₄, FeCl₃, AlCl₃, or ZnCl₂ (20 µM, final concentration) were recorded at room temperature for 30 min in buffer (dry methanol). For the stoichiometry of the compound-Cu²⁺ complex, the different concentrations of compounds **19n** or **20l** (0-100 µM) were mixed with CuCl₂ (100 µM), and the ratio of ligand/metal in the complex was investigated by the difference of UV-Vis spectrum.

4.2.5 ThT assay (Modulation of Cu²⁺-Induced Aβ Aggregation by Compound **19n**)

The procedure of ThT assay followed similar protocols from published studies [36]. Aβ₁₋₄₂ (MCE, HY-P1363) was dissolved in ammonium hydroxide (1% v/v) to give a stock solution (200 µM), which was aliquoted into small portions and stored at -80 °C. Aβ stock solution was diluted in 20 mM HEPES (pH 7.5) and 150 mM NaCl. The tested

compound (10 μ L, 50 M, final concentration) was combined with the peptide (10 μ L, 25 M, final concentration) with or without copper (10 μ L, 25 M, final concentration). This mixture was incubated at 37 °C for 24 hours. Then 20 μ L of the sample was diluted to a final volume of 200 μ L with 50 mM glycine NaOH buffer (pH 8.0) containing thioflavin T (20 μ M). Five minutes later, the fluorescence intensities were measured (excitation: 450 nm; emission: 485 nm). The expression, $(IF_i/IF_c) \times 100\%$, in which IF_i and IF_c are the fluorescence intensities obtained for $A\beta$ in the presence and absence of inhibitors after subtracting the background, respectively, was used to calculate the percentage of inhibition of aggregation.

4.2.6 TEM assay

The procedure of TEM assay followed similar protocols from published studies [36]. A stock solution was diluted with a 10 mM phosphate buffer (pH = 7.4) for the metal-free experiment; for the copper-induced experiment, it was diluted with a 20 mM HEPES (pH = 7.5) and 150 mM NaCl solution. The sample was prepared in the same manner as the ThT assay. The samples were divided into aliquots (10 μ L) and left on a carbon-coated copper/rhodium grid for 5 minutes. Phosphotungstic acid (1%, 10 μ L) was used to stain each grid and was left on for 5 minutes. The specimen was moved to a transmission electron microscope (JEOL, JEM-200CX) for imaging after the excess staining solution was drained off.

4.2.7 Quantification of AChE-induced $A\beta$ aggregation

Measurements of AChE-induced amyloid aggregation were taken following the protocol reported by Jiang et al [43]. Briefly, hexafluoroisopropanol (HFIP)-treated E22G $A\beta$ peptides (# SP-Ab-11_0.1, JPT – Innovative Peptide Solution) were dissolved in DMSO to reach a final 200 μ M stock. The dissolved peptides were subsequently centrifuged at 13500g for 10 minutes, the supernatant was then transferred into a fresh vial used for the following experiments. To evaluate the aggregation rate in presence of AChE inhibitors, 2 μ L of the compound of interest (at the appropriate concentration) were added into each vial, followed by 2 μ L of 200 μ M $A\beta$ peptides stock, 20 μ L AChE

enzyme (#C3389-500UN, Sigma-Aldrich ltd) (2 U/mL, in 1X PBS at pH 8.0), and 76 μ L of 1X PBS pH 8.0. The reaction was then incubated at RT for 24 hours. Subsequently, 100 μ L of 5 μ M Thioflavin T (ThT) was added to each vial. After one-hour incubation at RT, fluorescence emission was recorded at 490nm with an excitation wavelength of 450nm using a Tecan Spark microplate reader. Results were then processed as done by Jiang and colleagues using the subsequent formula: $(F_i - F_b) / (F_o - F_b) \times 100$. Where F_i corresponds to amyloid aggregation in presence of peptides, AChE, AChE inhibitors and ThT; F_o represents the amyloid aggregation in presence of peptides, AChE and ThT; F_b corresponds to blank control containing ThT only.

4.2.8 Cytotoxicity assay on SH-SY5Y cells.

3-(4,5-Dimethylthiazol-2-yl)-2,5-diphenyltetrazolium bromide (MTT) assay was performed to evaluate the cytotoxicity of donepezil and the optimal compound **19n** on SH-SY5Y cells. Briefly, the SH-SY5Y cells were dissociated with trypsin, inoculated in a 96-well plate at a density of 2×10^5 cells/mL and incubated overnight. The tested compound was dissolved in DMSO and gradually diluted to the desired test concentration in fresh MEM/F12 medium. 10 μ L of the tested compound was added to each well as the administration group, and the same volume of MEM/F12 medium was added to the control group. After incubated for 24 h, MTT solution was added to incubate for another 4h. Finally, removed the supernatant and added 100 μ L DMSO to each well, the absorbance value of each well was measured at 490 nm by the microplate reader (MULTISKAN FC, Thermo Scientific) after 20 min of vibration dissolution, and the survival rate was calculated by the following expression: $A_e/A_b \times 100\%$, where A_e and A_b are the absorbances obtained for SH-SY5Y cells in the presence and absence of the tested compounds, respectively. Each experiment was analyzed in triplicate.

4.2.9 Determination of intracellular AChE activity in SH-SY5Y cells

Ellman Method was used to evaluate intracellular AChE inhibition potential of test compound **19n**. 5,5-dithiobis-(2-nitrobenzoic acid) (DTNB) assay was based on the Ellman method in which thiocholine, produced by acetylcholinesterase, reacted with

DTNB to form a colorimetric product (412 nm), named 2-nitro-5-thiobenzoic acid (TNB), proportional to the Acetylcholinesterase activity present. Acetylcholinesterase activity was assessed using an acetylcholinesterase assay kit (#ab138871, Abcam plc.) following the manufacturer's instruction. Cells (100 μ L, 1×10^5 cells per well) were seeded into a 96-well plate and incubated for 24h at 37°C with 5% CO₂. After 24 hours of drug treatment, cell culture media was removed, and 100 μ L of lysis buffer (1% Triton X-100) was added to each well and left to incubate for 15 minutes at room temperature. Subsequently, 50 μ l of the acetylthiocholine reaction mixture (1X assay buffer, 1X DTNB stock solution, 1X acetylthiocholine stock solution) were added to each well and samples were left to incubate for 30 minutes at room temperature. Samples were then analyzed using a 96-well microplate reader at OD= 412 nm. To avoid false positive given by butyrylcholinesterase activity, the specific AChE inhibitor donepezil hydrochloride was used as the positive control.

4.2.10 Measurement of Mitochondrial Membrane Potential (MMP)

The cationic dye tetraethylbenzimidazolylcarbocyanine iodide (JC-1) accumulates in energized mitochondria. JC-1 aggregates in healthy cells with high MMP levels. JC-1, on the other hand, stays monomeric in cells with low MMP levels. As a result, a drop in the aggregate fluorescent count indicates depolarization and increased apoptosis. The mitochondrial membrane potential was measured by using JC-1 assay kit (#ab113850, Abcam plc). Culture cells in a 96-well black plate at a density of 3×10^4 cells/well in 100 μ l culture medium in a CO₂ incubator overnight at 37°C. After incubation, the cells were exposed to vehicle, Donepezil or **19n** for 24 h, then treated for a further 24h with 30nM okadaic acid. Following treatment, cells were washed once with PBS and then incubated with 20 μ M (final concentration) of JC-1 dye and incubated the cells at 37 °C, 5% CO₂ for 10 min. After incubation, the plate was washed twice with dilution buffer solution. Finally, the 96-well plate can be tested using a microplate reader. Green fluorescence was measured at wavelengths of 485 nm excitation and 535 nm emission, while red fluorescence was measured at 535 nm excitation and 595 nm emission.

4.2.11 Measurement of Intracellular ROS

Intracellular ROS levels were determined using 2',7'-dichlorofluorescein diacetate (DCFH-DA). When applied to intact cells, DCFH-DA crosses the cell membranes and is converted by intracellular esterase to non-fluorescent DCFH. However, in the presence of ROS, DCFH is oxidized to fluorescent dichlorofluorescein (DCF), which can be used to quantify intracellular ROS in the cells. SHSY-5Y cells were seeded at a density of 3×10^4 cells/well in a 96-well clear bottom plate and cultured for 24 h at 37°C with 5% CO₂. After 24 h the cells were exposed to vehicle, donepezil or **19n** for 24h, okadaic acid was added at 100 nM concentrations for 3 hours. And then, cells were incubated with 40 μM DCFH-DA for 30 mins at 37°C with 5% CO₂. The dye was removed, and cells were washed three times with PBS, 100 μL of fresh PBS was added to each well and fluorescence was measured using a microplate reader at wavelengths of 485 nm excitation and 535 nm emission.

4.2.12 Measurements of phosphorylated tau

SH-SY5Y cells were incubated in 6-well plates with a density of 3×10^5 cells/well. The **19n** and donepezil to be tested were co-incubated with GA for 24 h at 3 μM and 0.3 μM. Phosphorylated tau proteins were measured as follows: cells were dissolved in extraction buffer containing RIPA solution (1% Protease inhibitor and 1% phosphatase inhibitor), followed by incubation for 30min on ice. After being centrifuged (14000xg, 15min, 4°C), supernatants were applied to the ELISA kit. Intracellular protein concentrations were measured using Bradford ULTRA.

4.2.13 Acute Toxicity Studies

ICR mice (female, 8-10 weeks old, 18–20 g) purchased from Shanghai Institute for Biomedical and Pharmaceutical Technologies (Shanghai, China) were used to evaluate the acute toxicity of compounds **19n** and donepezil. Mice were maintained with a 12 h light/dark cycle (light from 07:00 to 19:00) at 20–26 °C with a 40–70% relative humidity. Following institutional guidelines, sterile food and water were provided. Mice were fasted for 24 hours and given free access to water before each experiment.

Compounds **19n** and donepezil were in suspension in 10% cyclodextrin solution (1200mg/kg for **19n**; 21.30, 26.62, 33.28, 41.60, and 52.00 mg/kg for donepezil) and given via oral administration according to the divided experimental groups. Any abnormal behavior and mortality changes were observed continuously for the first 4 hours after the compounds were administered, intermittently for the next 24 hours, and occasionally thereafter for 14 days for any delayed effects.

4.2.14 Morris water maze test in scopolamine-induced mice [43]

Adult female ICR mice (8-10 weeks, 25-30 g, Shanghai, China) were used as experimental subjects. The mice were randomly divided into 4 groups on average :(i) control group (physiological saline); (ii) model group (scopolamine); (iii) compound group (scopolamine + **19n**); (iv) positive group (scopolamine + donepezil). The experiment lasted 16 days and was divided into the following sections: (1) Injection phase (days 1-10): donepezil, **19n** (15 mg/kg) or saline was injected intraperitoneally once daily for 10 consecutive days, followed 30 min later by scopolamine solution (5 mg/kg). (2) Exploration phase (days 11-16): the water maze was placed in a darkened room at 25 °C. The circular pool (120 cm in diameter and 60 cm in height) was divided equally into 4 quadrants, with a 10 cm diameter escape platform in the center of the fourth quadrant and a water depth of 40 cm. The behavioral study of each mouse consisted of learning and memory training on days 11-14 and cognitive behavioral assessment on day 16, with the same daily injections of the appropriate drugs on these 5 days. The mice were placed in the pool and went to find the platform. Each mouse was trained once in each of the four quadrants of the pool (days 11-14) for 90 seconds, and the time it took for the mouse to find the platform (i.e. a successful escape) was recorded. If the mice failed to reach the platform within 90 seconds, the test was terminated by the mice being guided to the platform. The mice were kept on the platform for 10 seconds whether or not they successfully reached the platform within 90 seconds. On the final day (day 16), mice were subjected to an exploratory experiment (water entry from the second quadrant) in which they had 90 seconds to find the platform. Data on the time the mice reached the missing platform, the number

of times they crossed the platform position and the escape latency was recorded by ANY-maze video tracking system and analyzed and processed using GraphPad Prism 8.0 software.

4.2.15 Morris water maze and Y maze tests in oligomerized A β ₁₋₄₂-induced-mice

Oligomerized A β ₁₋₄₂-induced-mice were performed using the previously reported method with a minor revision [45]. Adult male C57bl/6 mice (8-10 weeks, 25-30g, Shanghai, China) were used as experimental subjects. Recombinant human 1,1,1,3,3,3-hexafluoro-2-propanol-pretreated A β ₁₋₄₂ (Beyotime, China) was dissolved in DMSO as a 5 mM stock solution and incubated for 24 h at 37 °C in normal saline at a final concentration of 2 mg/mL to induce A β ₁₋₄₂ aggregation. The mice were randomly divided into 4 groups on average (n = 15) : (i) control group (vehicle + vehicle); (ii) model group (vehicle + A β ₁₋₄₂); (iii) positive group (A β ₁₋₄₂ + donepezil); (iv) compound group (A β ₁₋₄₂ + **19n**). On the first day, oligomerized A β ₁₋₄₂ (10 μ g per mouse) was injected into the lateral ventricles of the mice, A β ₁₋₄₂ was injected only once in this experiment. On the fourth day, the experiment was the same to 4.13 to start the exploration phase. On the ninth day, the three-arm Y-maze apparatus was tested for immediate spatial working memory. Mice arms were thoroughly cleaned, wiped with 70% v/v ethanol and labeled as arms A, B and C. Mice were placed individually in the center of the maze. Spontaneous alternating behavior was recorded for a total of 10 minutes. Mice were considered to have entered the arm when all four paws straddled the arm. An increase in the number of spontaneous alternations was considered to be an indicator of improved learning and memory. The percentage of duration in the novel arm was calculated according to the following expression. [number of spontaneous alternations / (total arm entries - 2)] \times 100.

4.2.16 The abundance of interleukin-1 β (IL-1 β) and tumor necrosis factor- α (TNF- α) in cortex

The levels of IL-1 β and TNF- α were detected using ELISA kits (Elabscience, Wuhan, China) by following the manufacturer's instructions.

Acknowledgments

This study was supported from the National Natural Science Foundation of China (nos. 81874289 and 81903446), The Open Project of State Key Laboratory of Natural Medicines, China Pharmaceutical University (SKLNMKF 201710), the Natural Science Foundation of Jiangsu Province (BK20190564), the China Postdoctoral Science Foundation Grant 2019M652037, and “Double First-Class” University project (nos. CPU2018GY04, CPU2018GY35), China Pharmaceutical University. This study was also funded by School of Pharmacy, The University of Nottingham (RJ/T5433).

ABBREVIATIONS

$A\beta$, β -amyloid; ACh, acetylcholine; AChE, acetylcholinesterase; AChEIs, AChE inhibitors; AD, Alzheimer’s disease; BBB, blood-brain barrier; PAS, peripheral anionic site; CAS, catalytic anionic site; MTDLs, multi-target-directed ligands; (\pm)-XJP, (\pm)-7,8-Dihydroxy-3-methyl-isochroman-4-one; OA, okadaic acid; ELISA, enzyme linked immunosorbent assay; GA, glyceraldehyde; ROS, reactive oxygen species; MMP, mitochondrial membrane potential; HPLC, high-performance liquid chromatography; HRMS high-resolution mass spectrometry; MTT, Thiazolyl blue; MWM, Morris water maze; NFTs, neurofibrillary tangles; NMDA, *N*-methyl-D-aspartate; PAS, peripheral anionic site; PBS, phosphate buffer saline; PBS-T, PBS in Tween-20; p-Tau, phosphorylated tau protein; S199, serine-199; S396, serine-396; SARs, structure-activity relationships; SP, senile plaques; THF, tetrahydrofuran; ThT, Thioflavine-T; TLC, thin-layer chromatography; Don, donepezil; CQ, Clioquinol transmission; TEM, electron microscopy; IL-1 β , interleukin-1 β ; TNF- α , tumor necrosis factor- α .

REFERENCES

- [1] L. Zhang, C. Chen, M.S. Mak, J. Lu, Z. Wu, Q. Chen, Y. Han, Y. Li, R. Pi, Advance of sporadic Alzheimer's disease animal models, *Med. Res. Rev.* 40 (2020) 431-458.
- [2] Alzheimer’s Association, 2020 Alzheimer's disease facts and figures, *Alzheimers Dement.* 16 (2020) 391-460.

- [3] A. Abramov, S. Bachurin, Neurodegenerative disorders-Searching for targets and new ways of diseases treatment, *Med. Res. Rev.* 41 (2021) 2603-2605.
- [4] S. Devenish, The current landscape in Alzheimer's disease research and drug discovery, *Drug Discov. Today.* 25 (2020) 943-945.
- [5] C.R. Jack, D.M. Holtzman, Biomarker Modeling of Alzheimer's Disease, *Neuron.* 80 (2013) 1347-1358.
- [6] Q. Sun, N. Xie, B. Tang, R. Li, S. Yong, Alzheimer's Disease: From Genetic Variants to the Distinct Pathological Mechanisms, *Front Mol Neurosci.* 10 (2017) 319.
- [7] T. Umar, N. Hoda, Alzheimer's Disease: A Systemic Review of Substantial Therapeutic Targets and the Leading Multi-functional Molecules, *Curr. Top. Med. Chem.* 18 (2018) 3370-3389.
- [8] M. Rossi, M. Freschi, L. de Camargo Nascente, A. Salerno, S. de Melo Viana Teixeira, F. Nachon, F. Chantegreil, O. Soukup, L. Prchal, M. Malaguti, C. Bergamini, M. Bartolini, C. Angeloni, S. Hrelia, LA. Soares Romeiro, ML. Bolognesi, Sustainable Drug Discovery of Multi-Target-Directed Ligands for Alzheimer's Disease, *J. Med. Chem.* 64 (2021) 4972-4990.
- [9] A. Kurz, R. Perneczky, B. Psychiatry, Novel insights for the treatment of Alzheimer's disease, *Prog. Neuropsychopharmacol Biol. Psychiatry.* 35 (2011) 373-379.
- [10] M. Singh, M. Kaur, H. Kukreja, R. Chugh, O. Silakari, D. Singh, Acetylcholinesterase inhibitors as Alzheimer therapy: From nerve toxins to neuroprotection, *Eur. J. Med. Chem.* 70 (2013) 165-188.
- [11] H. Yao, G. Uras, P. Zhang, S. Xu, Y. Yin, J. Liu, S. Qin, X. Li, S. Allen, R. Bai, Q. Gong, H. Zhang, Z. Zhu, J. Xu, Discovery of Novel Tacrine-Pyrimidone Hybrids as Potent Dual AChE/GSK-3 Inhibitors for the Treatment of Alzheimer's Disease. *J. Med. Chem.* 64 (2021) 7483-7506.
- [12] E.J. Barreiro, C.A. Camara, H. Verli, L. Brazilmás, N.G. Castro, W.M. Cintra, Y. Aracava, C.R. Rodrigues, C. Fraga, Design, synthesis, and pharmacological profile of novel fused pyrazolo[4,3-d]pyridine and pyrazolo[3,4-b][1,8]naphthyridine isosteres: a new class of potent and selective acetylcholinesterase inhibitors, *J. Med. Chem.* 46 (2003) 1144-1152.

- [13] K. Blennow, M. Leon, H. Zetterberg, Alzheimer's disease, *Lancet*. 368 (2006) 387-403.
- [14] D.G. van Greunen, C. Johan van der Westhuizen, W. Cordier, M. Nell, A. Stander, V. Steenkamp, J.L. Panayides, D.L. Riley, Novel N-benzylpiperidine carboxamide derivatives as potential cholinesterase inhibitors for the treatment of Alzheimer's disease, *Eur. J. Med. Chem.* 179 (2019) 680-693.
- [15] R. Saini and A. Saxena, The Structural Hybrids of Acetylcholinesterase Inhibitors in the Treatment of Alzheimer's Disease: A Review, *J Alzheimers Dis.* (2018).
- [16] P. Zhang, S. Xu, Z. Zhu, J. Xu, Multi-target design strategies for the improved treatment of Alzheimer's disease, *Eur. J. Med. Chem.* 176 (2019) 228-247.
- [17] A. Gschwind, E. Zwick, N. Prenzel, M. Leserer, A. Ullrich, Cell communication networks: epidermal growth factor receptor transactivation as the paradigm for interreceptor signal transmission, *Oncogene*. 20 (2001) 1594-1600.
- [18] K.P. Kepp, Bioinorganic Chemistry of Alzheimer's Disease, *Chem. Rev.* 112 (2012) 5193-5239.
- [19] A.I. Bush, The Metal Theory of Alzheimer's Disease, *J. Alzheimers Dis.* 33 (2013) S277-S281.
- [20] M.G. Savelieff, S. Lee, Y. Liu, M.H. Lim, Untangling Amyloid- β , Tau, and Metals in Alzheimer's Disease, *ACS Chem. Biol.* 8 (2013) 856-865.
- [21] E. Gumienna-Kontecka, M. Pyrkosz-Bulska, A. Szebesczyk, M. Ostrowska, Iron Chelating Strategies in Systemic Metal Overload, Neurodegeneration and Cancer, *Curr. Med. Chem.* 21 (2014) 3741-3767.
- [22] S. Rivera-Mancía, I. Pérez-Neri, C. Ríos, L. Tristán-López, L. Rivera-Espinosa, S. Montes, The transition metals copper and iron in neurodegenerative diseases, *Chem. Biol. Interact.* 186 (2010) 184-199.
- [23] A. Agis-Torres, M. Slhuber, M. Fernandez, J.M. Sanchez-Montero, Multi-Target-Directed Ligands and other Therapeutic Strategies in the Search of a Real Solution for Alzheimer's Disease, *Curr. Neuropharmacol.* 12 (2014) 2-36.

- [24] M.J. Oset-Gasque, J. Marco-Contelles, *Neuroscience, Alzheimer's Disease, the "One-Molecule, One-Target" Paradigm, and the Multitarget Directed Ligand Approach*, *ACS Chem. Neurosci.* 9 (2018) 401-403.
- [25] J. Yan, J.H. Hu, A.Q. Liu, L. He, X.S. Li, H. Wei, Design, synthesis, and evaluation of multitarget-directed ligands against Alzheimer's disease based on the fusion of donepezil and curcumin, *Bioorg. Med. Chem.* 25 (2017) 2946-2955.
- [26] J. Liu, H. Ren, J. Xu, R. Bai, Q. Yan, W. Huang, X. Wu, J. Fu, Total synthesis and antihypertensive activity of (\pm)-7,8-dihydroxy-3-methyl-isochromanone-4, *Bioorg. Med. Chem. Lett.* 19 (2009) 1822-1824.
- [27] R. Fu, T. Yan, Q. Wang, Q. Guo, H. Yao, X. Wu, Y. Li, Suppression of endothelial cell adhesion by XJP-1, a new phenolic compound derived from banana peel, *Vascul Pharmacol.* 57 (2012) 105-112.
- [28] R. Fu, Q. Wang, Q. Guo, J. Xu, X. Wu, XJP-1 protects endothelial cells from oxidized low-density lipoprotein-induced apoptosis by inhibiting NADPH oxidase subunit expression and modulating the PI3K/Akt/eNOS pathway. *Vascul Pharmacol.* 58 (2013) 78-86.
- [29] R. Bai, X. Yang, Y. Zhu, Z. Zhou, W. Xie, H. Yao, J. Jiang, L. Jie, M. Shen, X. Wu, J. Xu, Novel nitric oxide-releasing isochroman-4-one derivatives: Synthesis and evaluation of antihypertensive activity, *Bioorg. Med. Chem.* 20 (2012) 6848-6855.
- [30] C. Wang, Z. Wu, H. Cai, S. Xu, J. Liu, J. Jiang, H. Yao, X. Wu, J. Xu. Design, synthesis, biological evaluation and docking study of 4-isochromanone hybrids bearing N-benzyl pyridinium moiety as dual binding site acetylcholinesterase inhibitors, *Bioorg. Med. Chem. Lett.* 25 (2015), 5212-5216.
- [31] J. Wang, C. Wang, Z. Wu, X. Li, S. Xu, J. Liu, Q. Lan, Z. Zhu, J. Xu, Design, synthesis, biological evaluation, and docking study of 4-isochromanone hybrids bearing N-benzyl pyridinium moiety as dual binding site acetylcholinesterase inhibitors (part II), *Chem. Biol. Drug Des.* 91 (2018) 756-762.
- [32] W. Shuai, W. Li, Y. Yin, L. Yang, F. Xu, S. Xu, H. Yao, Z. Zhu, J. Xu, Design, synthesis and molecular modeling of isothiochromanone derivatives as acetylcholinesterase inhibitors, *Future Med. Chem.* 11 (2019) 2687-2699.

- [33] G. Uras, A. Manca, P. Zhang, Z. Markus, N. Mack, S. Allen, M. Bo, S. Xu, J. Xu, M. Georgiou, Z. Zhu, In vivo Evaluation of a Newly Synthesized Acetylcholinesterase Inhibitor in a Transgenic *Drosophila* Model of Alzheimer's Disease. *Front. Neurosci.* 15 (2021) 691222.
- [34] M. G. Savelieff, G. Nam, J. Kang, H. J. Lee, M. Lee, M. H. Lim, Development of Multifunctional Molecules as Potential Therapeutic Candidates for Alzheimer's Disease, Parkinson's Disease, and Amyotrophic Lateral Sclerosis in the Last Decade. *Chem. Rev.* 119 (2019), 1221-1322.
- [35] G. L. Ellman, K. D. Courtney, V.A. Jr., R. M. Feather-Stone, A new and rapid colorimetric determination of acetylcholinesterase activity. *Biochem. Pharmacol.* (7) (1961), 88-95.
- [36] Z. Wang, Y. Wang, B. Wang, W. Li, L. Huang, X. Li, Design, Synthesis, and Evaluation of Orally Available Clioquinol-Moracin M Hybrids as Multitarget-Directed Ligands for Cognitive Improvement in a Rat Model of Neurodegeneration in Alzheimer's Disease, *J. Med. Chem.* 58 (2015) 8616-8637.
- [37] P. K. Kamat, S. Tota, R. Shukla, S. Ali, A. K. Najmi, C. Nath, Mitochondrial dysfunction: a crucial event in okadaic acid (ICV) induced memory impairment and apoptotic cell death in rat brain. *Pharmacol. Biochem. Behav.* 100 (2011), 311-319.
- [38] Y. Koriyama, A. Furukawa, M. Muramatsu, J. T. Takino, Glyceraldehyde caused Alzheimer's disease-like alterations in diagnostic marker levels in SH-SY5Y human neuroblastoma cells. *Sci. Rep.* 5 (2015), 13313.
- [39] H. Zhang, Y. Wang, Y. Wang, X. Li, S. Wang, Z. Wang, Recent advance on carbamate-based cholinesterase inhibitors as potential multifunctional agents against Alzheimer's disease, *Eur. J. Med. Chem.* 240 (2022) 114606.
- [40] J. Guo, M. Cheng, P. Liu, D. Cao, J. Luo, Y. Wan, Y. Fang, Y. Jin, S.S. Xie, J. Liu, A multi-target directed ligands strategy for the treatment of Alzheimer's disease: Dimethyl fumarate plus Tranilast modified Dithiocarbamate as AChE inhibitor and Nrf2 activator, *Eur. J. Med. Chem.* 242 (2022) 114630.
- [41] W. Liu, L. Wu, W. Liu, L. Tian, H. Chen, Z. Wu, N. Wang, X. Liu, J. Qiu, X. Feng, Z. Xu, X. Jiang, Q. Zhao, Design, synthesis and biological evaluation of novel coumarin

derivatives as multifunctional ligands for the treatment of Alzheimer's disease, Eur. J. Med. Chem. 242 (2022) 114689.

[42] B. Turgutalp, P. Bhattarai, T. Ercetin, C. Luise, R. Reis, E.E. Gurdal, A. Isaak, D. Biriken, E. Dinter, H. Sipahi, D. Schepmann, A. Junker, B. Wünsch, W. Sippl, H.O. Gulcan, C. Kizil, M. Yarim, Discovery of Potent Cholinesterase Inhibition-Based Multi-Target-Directed Lead Compounds for Synaptoprotection in Alzheimer's Disease, J. Med. Chem. 65 (2022) 12292-12318.

[43] N. Jiang, J. Ding, J. Liu, X. Sun, Z. Zhang, Z. Mo, X. Li,; H. Yin, W. Tang, S. S. Xie, Novel chromanone-dithiocarbamate hybrids as multifunctional AChE inhibitors with β -amyloid anti-aggregation properties for the treatment of Alzheimer's disease. Bioorg. Chem. 89 (2019), 103027.

[44] C. Zhang, K. Yang, S. Yu, J. Su, S. Yuan, J. Han, Y. Chen, J. Gu, T. Zhou, R. Bai, Y. Xie, Design, synthesis and biological evaluation of hydroxypyridinone-coumarin hybrids as multimodal monoamine oxidase B inhibitors and iron chelates against Alzheimer's disease, Eur. J. Med. Chem. 180 (2019) 367-382.

[45] Q. Li, Y. Chen, S. Xing, Q. Liao, B. Xiong, Y. Wang, W. Lu, S. He, F. Feng, W. Liu, Y. Chen, H. Sun, Highly Potent and Selective Butyrylcholinesterase Inhibitors for Cognitive Improvement and Neuroprotection. J. Med. Chem. 64 (2021), 6856-6876.